Graduate School of Bioresources
Mie University

Ph.D. Thesis

Evaluation of the effects of mutation in the wheat *AP2* homoeologs on the potential for cleistogamous flowering

（コムギ *AP2* 同祖遺伝子変異が閉花受粉性の獲得に及ぼす効果の評価）

Nanape Agetha Bigie

July 2024

Contents

Publication

Chapter II was published as a research paper in the following journal:

Nanape AB, Haine HM, Sugimoto K, Kobayashi F, Oono Y, Handa H, Komatsuda T, Kakeda K

Mutations within the miR172 target site of wheat *AP2* homoeologs regulate lodicule size and rachis internode length.

Breeding Science 71: 401-407 (2023)

https://doi.org/10.1270/jsbbs.23019

Chapter III was published as aa original paper in the following journal:

Nanape AB, Komatsuda T, Kakeda K

Accumulation of mutations in the *AP2* homoeologs causes suppression of anther extrusion with altered spike and culm development in hexaploid wheat.

Molecular Breeding 44, 19 (2024)

https://doi.org/10.1007/s11032-024-01458-9

Chapter I

General introduction

Wheat (*Triticum aestivum*) has been a fundamental and essential crop in the global food industry since the inception of human civilization. With its cultivation covering a substantial land area, ranking third among grain crops after rice and maize (FAO 2015). This crop is a valuable source of energy, protein, starch and minerals, and is used in a variety of food products for human consumption (Sparks et al. 2004). It is also used as animal feed, industrial raw materials and biofuels. Wheat consumption is a significant part of the global diet, with approximately 630 million tons produced annually (Mehta 2014). Global wheat production has been steadily increasing, with 723 million tons produced in 2014/2015 (Purnell 2016). The global wheat area is 221.7 million hectares, with an average yield of 2977 kg per hectare and a production of 660 million tonnes (He et al. 2013). This is expected to rise to 840 million tons by 2050 (Sharma et al. 2015). It is projected that the demand for wheat will continue to increase, particularly in developing countries (He et al. 2013). Despite these increases, the industry faces challenges such as disease threats and the need for sustainable production (Sharma et al. 2015, Guarin et al. 2022). The primary goal of crop domestication and breeding programs is to improve grain yield, which depends on inflorescence architecture (Wang et al. 2017).

However, wheat production can be hampered by diseases like Fusarium head blight (FHB) or scab which is mainly caused by *Fusarium graminearum* and is one of the most destructive fungal diseases of wheat (Beccari et al. 2019). FHB has a

considerable influence on winter wheat production and quality (Cosic et al. 2008). The pathogen infects spikes and higher infection levels lead to reduced wheat yield, test weight, thousand kernel weight and grain quality with the severity of the impact varying among cultivars (Cosic et al. 2008, Salgado et al. 2011). The disease affects the number of grains per spike, leading to a decrease in yield (Kadar et al. 2012). FHB is a significant threat to wheat production, causing economic losses and health risks (Salgado et al. 2015, Wegulo et al. 2015). The disease also affects grain characteristics, including deoxynivalenol (DON) content, which varies based on location, harvest year and cultivar (Polisenska et al. 2020). Fusarium-infected wheat kernels accumulate DON and nilvalenol (NIV) throughout grain development stages, posing a risk to both human and animal health (Yoshida and Nakajima 2010). Although the disease can occur anytime during flowering time and kennel development, it is more frequent during flowering time because anthers provide stimulants for spore germination and pathogen growth (Alisaac et al. 2021). Protection measures such as fungicide application and selection of less susceptible cultivars are crucial in mitigating the negative effects of FHB on yield and grain quality (Ćosić et al. 2008, Bekele et al. 2018). However, the frequent use of agricultural chemicals for prevention has negative environmental and health impacts (Hollingsworth et al. 2008). In addition, the influence of tillage and fertilization practices on FHB infection and mycotoxin production in wheat grains is less clear, with some studies showing no significant impact (Suproniene et al. 2012). The use of seed treatment fungicides and higher seedling rates can reduce FHB symptoms and DON accumulation, but the relationship between these factors and the disease is complex (Schaafsma et al. 2005). One of the most important approaches to achieving stable yield production while reducing costs for fungicide application is the development of FHB resistant or tolerant cultivars.

Cleistogamy, the trait of non-opening flowers, is a type of sexual reproduction system where pollination and fertilization process take place in an unopened (closed) flower, whereas chasmogamy occurs in opened flowers (Fig. I-1a). Cleistogamy offers advantages such as adaptability in adverse conditions, reduction of pollen-mediated gene flow in genetically modified (GM) crops and lowering FHB causal fungi infection in barley and wheat, making it valuable for disease control (Yoshida et al. 2007, Ni et al. 2014). These properties make cleistogamy an important and useful agronomic trait for grass species, especially wheat.

Barley (*Hordeum vulgare*) exhibits both cleistogamous and chasmogamous flowering. In cleistogamous barley, the flower sheds its pollen without opening and therefore self-fertilized. Cleistogamous barley exhibits greater FHB causal fungi resistance than chasmogamous barley (Yoshida et al. 2007, Kubo et al. 2010). The identification and utilization of cleistogamy genes in rice have also been explored, with the potential to improve agronomic traits and prevent transgene propagation (Ni et al. 2014). Cleistogamous rice lines have been shown to effectively inhibit natural crossing without significant loss of commercial benefits (Ohmori et al. 2012). In oilseed rape, cleistogamy has been found to limit pollen dispersal and reduce gene flow, making it a potential tool for gene containment in GM crops (Pierre et al. 2007, Leflon et al. 2011).

Barley's cleistogamy is controlled by a single recessive gene, *cleistogamy 1* (*cly1*), which is mapped to the long arm of chromosome 2H (Turuspekov et al. 2004). The *Cly1* gene was isolated by map-based cloning, and was found to encode an AP2 transcription factor, HvAP2 (Nair et al. 2010). The down-regulation of *Cly1* by microRNA172 (miR172) allows normal lodicule development in wild-type (chasmogamous) barley. The cleistogamous *cly1* allele contains a single nucleotide polymorphism (SNP) which lies within a 21-nucleotide sequence in the miR172 target

site (Fig. I-1b). The point mutation inhibits the binding of miR172 with its mRNA and this leads to the expression of *HvAP2*, which is assumed to negatively regulate lodicule development and causing closed flowering during anthesis. The lodicule size and auxin response are key factors in this process, with the cleistogamy gene playing a role in auxin response or metabolism (Honda et al. 2005). Morphologically, cleistogamous flowers have smaller lodicules than chasmogamous flowers (Nair et al. 2010).

Wheat *AP2* genes (*TaAP2*s) are categorized into three groups, euAP2, euANT and basalANT, where they all contain two highly conserved AP2 domains together with other various motifs. However, euAP2 is the only group that contains motif 16, which is responsible for the miR172 targeting site (Zhao et al. 2019). Common wheat (*T. aestivum*) is hexaploid and consists of A, B and D subgenomes and is thus represented as the genome symbol, AABBDD. Each subgenome contains 7 homoeologous chromosomes where each orthologous gene generally exists in triplicate and known as 'homoeologs'. In hexaploid wheat, three homoeologous orthologs of the barley *Cly1* gene, *TaAP2-A*, *TaAP2-B* and *TaAP2-D* have all been cloned by screening of BAC clones (Ning et al. 2013a). The three homoeologs, hereafter referred to as *AP2-A*, *AP2-B* and *AP2-D*, have a structure and transcription pattern similar to that of *Cly1* in barley. The miR172 target site was conserved in each wheat *AP2* homoeolog which is highly similar in sequence to that of *Cly1* and phylogenetically related to one another.

The point mutation within the miR172 target site not only regulates lodicule development but also has pleiotropic effects on other agronomic traits including spike architecture, plant height, rachis internode length, biomass, tiller number and free threshing grains, and grain related traits (Houston et al. 2013, Debernardi et al. 2017, 2020, Xie et al. 2018). The *Q* gene in wheat, located on the long arm of chromosome 5A (Faris et al. 2002) encodes an AP2-like transcription factor that influences spike

morphology and threshability (Simons 2006) and has been found to be regulated by miR172 (Debernardi et al. 2017). A nucleotide change in the miR172 target site of the *Q* gene can lead to compact spikes and a transition from glumes to florets in the apical spikelets when miR172 activity is inhibited, or to elongated spikes and non-free threshing grains when miR172 is overexpressed (Debernardi et al. 2017). The *Q* gene, a major wheat domestication gene, controls threshability, rachis fragility and spike shape traits (Sormacheva et al. 2014). According to Zhao et al (2018), a mutation within the miR172 target site of the *Q* gene has been linked to increased transcript levels, resulting in pleiotropic effects on spike compactness and plant dwarfness.

The wheat *AP2* homoeologs are highly expressed in floral organs, particularly lodicules. Lodicules are a pair of structures that are formed at the base of many grasses' floret between the lemma, palea and stamens (Yoshida 2012). The expansion of the lodicules pushes apart the palea and lemma and allows anthers to be extruded during anthesis. While lodicules are considered whorl 2 organs, similar to petals, their differences suggest that they may represent either a counterpart or a distinct type of organ not found in eudicot flowers (Yoshida 2012). A wide range of germplasms of wheat and its relatives, including diploid, tetraploid, and hexaploid species were investigated (Ning et al. 2013b). These accessions displayed a common flowering characteristic similar to barley, where lodicule swelling pushes open the lemma and palea, exposing the stigma and style at anthesis. Sequence analysis confirmed that the miR172 targeting site of each *AP2* homoeolog was highly conserved even across different ploidy levels. However, no natural variation was detected in each miR172 targeting site, despite screening a wide range of wheat accessions. Complete cleistogamy, comparable to that in barley, has not so far been found in any of the wheat accessions including hexaploid wheat. Assuming that a hypothetical mechanism of cleistogamy based on *cly1* gene in barley would be

applicable to cleistogamy in wheat, a possible strategy for engineering cleistogamous wheat is to accumulate point mutations within the miR172 target site from all three *AP2* homoeologs into one plant. According to Tang et al (2019), a wheat mutant, named *ZK001* was characterized as cleistogamy due to its inability to push apart the lemma and palea during flowering due to thin lodicules. Another cultivar 'U24' was once described as cleistogamous wheat (Ueno and Itoh 1997, Kubo et al. 2010). However, it has been re-evaluated and found to have swollen lodicule and that the florets were able to open partially. It is unlikely that mutations in *ZK001* and 'U24' are associated with the *AP2* gene.

Based on the above research background, this dissertation was conducted with a focus on the following two perspectives. Firstly, **Chapter II** focuses on the identification of novel mutations that were induced within the miR172 target site in the wheat *AP2* homoeologs using EMS mutagenesis. Three point mutations were identified in *AP2-A* and *AP2-D* genes, resulting in one mutant allele in *AP2-A* and two alleles in *AP2-D*, although no point mutations were detected in *AP2-B*. Their effects on lodicule development and spike architecture were evaluated. Next, in **Chapter III**, the effects of the mutations were evaluated in detail using near isogenic lines (NILs). In addition to NIL lines of three single mutants, double mutants of *AP2-A* and *AP2-D* were generated to test the accumulation effect of two mutated homoeologs in hexaploid wheat on flowering, spike and culm development, and other agronomic traits under a near-isogenic background.

(a)

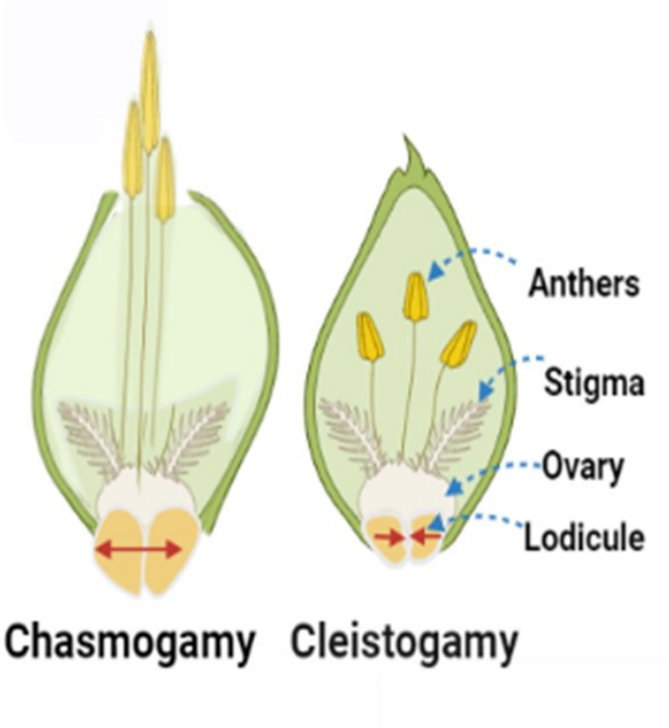

(b)

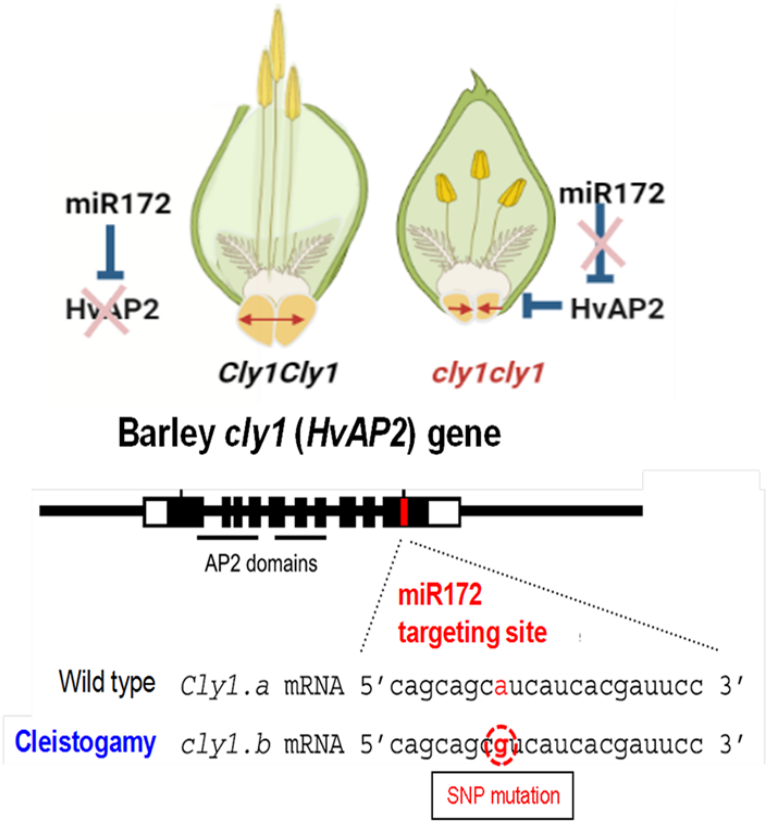

Fig. I-1 Cleistogamy and its function

(a) Cleistogamy (closed) and chasmogamy (open) types of flowering

(b) Model of the mechanism of barley cleistogamy

Chapter II

Mutations within the miR172 target site of wheat *AP2* homoeologs regulate lodicule size and rachis internode length

Introduction

Flowers in many grass species open as the swelling lodicules push apart the lemma and palea at anthesis. Open flowering, called chasmogamy, is the primary type of flowering in wheat (*Triticum aestivum*), barley (*Hordeum vulgare*), and other species. Some cultivars of barley, however, flower by cleistogamy (closed flowering at pollination/fertilization). In cleistogamous flowering, the lodicules are rudimentary and do not swell, so the floret remains closed. Cleistogamy in barley is determined by a single gene at the *Cleistogamy 1* (*cly1*) locus on chromosome 2H (Turuspekov et al. 2004). The *Cly1* gene encodes HvAP2, a barley ortholog of the *Arabidopsis* Apetala2 (AP2) transcription factor protein, and *Cly1* mRNA contains a microRNA172 (miR172) target site in the region of the 10th exon (Nair et al. 2010). Cleistogamous barley is homozygous for one of two recessive *cly1* alleles (*cly1.b*, *cly1.c*), which are natural variants each carrying a synonymous single nucleotide polymorphism (SNP) within the miR172 target site. The nucleotide change inhibits the binding of miR172 to the target site of *Cly1* mRNA in the lodicule and leads to production of the HvAP2 protein, which is assumed to negatively regulate lodicule development (Anwar et al. 2018).

Cleistogamous barley cultivars have been used in breeding programs, consciously or unconsciously, as they offer the advantage of evading infection by the fungus causing Fusarium head blight (FHB). The tests using spray inoculation of *Fusarium graminearum* clearly showed a clear difference in FHB severity between cleistogamous and chasmogamous barley lines, and revealed the contribution of cleistogamy toward FHB resistance more than that of row type and the other tested spike characters (Yoshida et al. 2005). Further survey on the effect of infection timing also indicated that cleistogamous barley cultivars were resistant at anthesis but susceptible at 10 days after anthesis, whereas chasmogamous cultivars were already susceptible at anthesis (Yoshida et al. 2007). Based on these findings in barley, Ning et al. (2013a) have attempted to

isolate wheat orthologs of the barley *Cly1* (*HvAP2*) gene as rational targets for engineering cleistogamy in wheat and successfully cloned three *AP2* homoeologs (designated *AP2-A*, *-B*, and *-D*) from hexaploid wheat. Natural sequence variations within their miR172 target site have been sought in a wide range of diploid, tetraploid, and hexaploid wheat accessions. However, the sequences of wheat *AP2* homoeologs are highly conserved across ploidy levels, and no sequence variant within the miR172 target site has been detected in any homoeolog (Ning et al. 2013b). The aim of this study was to isolate mutants carrying a novel point mutation within the miR172 target site in wheat *AP2* homoeologs. Here, we induced and identified such point mutations, and analyzed the lodicule and other spike traits of the mutants.

Materials and methods

Plant materials

The *AP2* mutants analyzed in this study were induced from the Japanese winter wheat cultivar 'Kitahonami'. Mutants carrying a point mutation within the miR172 target site were screened among 2157 M_2 individuals generated by single-seed descent from M_1 plants obtained from seeds treated with 0.5%, 0.7% or 0.75% ethyl methanesulfonate (EMS) solution for 18 h. Mutant plants were isolated by high-resolution melt (HRM) analysis, described next. In addition, null (deletion) mutants were screened from another M_2 population consisting of 1440 individuals that were generated by gamma-irradiation at 250 Gy, as described in Komura et al. (2022). Gene-specific PCR was used for each *AP2* homoeolog. All mutant lines of interest were maintained by selfing and the selection of good-fertility plants with no apparent growth defects. M_4 and M_5 plants were grown in the field for trait and expression analysis.

Screening of mutants and molecular analysis with genomic DNA

Genomic DNA was extracted by the CTAB method from the leaves of M_2 individuals and the parental cultivar. Mutants were screened for a SNP within the miR172 target site by HRM analysis using gene-specific primers for each *AP2* homoeolog (Table II-1, Ning et al. 2013a) in a ViiA 7 system (Applied Biosystems, Tokyo) with a MeltDoctor HRM Reagent Kit (Thermo Fisher Scientific, Tokyo) according to the manufacturers' instructions. Amplicons of HRM-positive mutants were Sanger-sequenced to identify the positions of the SNPs. For genotyping of M_3 plants derived from heterozygous M_2 mutants and for confirming mutants from M_4 onward, genomic DNA was extracted by the SDS method (Komatsuda et al. 1998) and sequenced. A complete DNA sequence (ca. 2.8 kbp) encompassing the coding region of the *AP2-A* or *AP2-D* gene was determined according to Ning et al. (2013b). Null mutants were screened by PCR amplification using the same gene-specific primers for each *AP2* homoeolog as described above (Table II-1, Ning et al. 2013a), followed by agarose gel electrophoresis.

RNA extraction and expression analysis

Total RNA was extracted from immature spikes harvested at the terminal spikelet stage or the white anther stage (Kirby and Appleyard 1981) with an RNeasy Mini Kit (Qiagen, Tokyo) according to Wang et al. (2021). Extracted RNA treated with RNase-

free DNase I (Qiagen) was used for cDNA synthesis with a High-Capacity RNA-to-cDNA Kit (Thermo Fisher Scientific). Quantitative real-time PCR (qRT-PCR) analysis was performed on a StepOnePlus Real-Time PCR System (Applied Biosystems) with Thunderbird SYBR qPCR Mix (Toyobo, Osaka) according to the manufacturers' protocols. The analysis used the ΔΔCt method (Livak and Schmittgen 2001) with 3′-UTR primers for each *AP2* homoeolog and the wheat *actin* gene as an internal control (Table II-1, Ning et al. 2013a). Each genotype was assayed as two biological replicates.

Measurement of lodicule size and spike density

On the day of anthesis, the culm below the flag leaf node was cut and held in water in a test tube at room temperature. Just before anthesis, the first, second or both florets were detached from a spikelet and the lemma was removed. The length, width and depth of each lodicule were measured (Fig. II-1) under a stereomicroscope with a DFC300 FX digital microscope camera system (Leica Microsystems, Tokyo). About 30 lodicules from 15–27 spikes per genotype were measured.

Using mature (or close to mature) spikes, the rachis length (i.e., the length of the central axis of a spike) was measured and the rachis nodes were counted, and the mean rachis internode length was calculated as an indicator of spike density.

Lodicule size and rachis traits were analyzed by one-way ANOVA, followed by Tukey's honestly significant difference for multiple comparison ($P < 0.05$).

Prediction of interaction between miR172 and target mRNA using RNAhybrid

The interaction of miR172 to the target site in the wild-type and mutant alleles of wheat *AP2* homoeologs was predicted using an online tool RNAhybrid as described in Rehmsmeier et al. (2004). RNAhybrid is an advanced algorithm that predicts the secondary structure of two RNA sequences, miRNA and target mRNA, by optimizing their hybridization in terms of minimum free energy (mfe). It extends the classical RNA secondary structure prediction algorithm and utilizes Dynamic Programming technique to calculate mfe. In the present analysis, the mature sequence of *miR172a* was used for wheat (*TamiR172a*, Ning et al. 2013a) and barley (*Hv-miR172a*, Anwar et al. 2018), based on the finding obtained in barley that miR172a is the most abundant in immature spikes among the three isomers (miR172a, b and c) and act to reduce the abundance of Cly1 (HvAP2) protein (Anwar et al. 2018). mRNA sequences from wheat *AP2* alleles along with barley *HvAP2* alleles were utilized as the targets.

Results

Screening of mutants

Four M_2 plants carrying a SNP within the miR172 target site were isolated by HRM analysis: 038E (carrying *AP2-A1* as described next), 156E and 514E (*AP2-D1*), and 190E (*AP2-D2*). Plants 038E, 156E, and 514E were heterozygous and 190E was homozygous for the mutation. Although 156E and 514E shared the same SNP, only 514E was selected for analysis because 156E and its progeny showed apparent growth defects. SNPs within the miR172 target site of *AP2-B* were not detected. Gene-specific PCR for each *AP2* homoeolog identified three null mutants, namely 1131A (*AP2-A*), 169B (*AP2-B*), and 248D (*AP2-D*) (Fig. II-2).

Identification of novel SNPs within the miR172 target site of wheat AP2 homoeologs

Three independent novel SNPs within the miR172 target site were identified, and were designated *AP2-A1*, *AP2-D1*, and *AP2-D2* (Fig. II-3). The position and nucleotide change of *AP2-A1* and *AP2-D1* were identical within the miR172-targeted 21-nt sequences, with a C-to-T change at the 7th nucleotide position. *AP2-D2* had a G-to-A nucleotide change at the 6th position. These SNPs are distinct from those identified in the cleistogamous alleles *cly1.b* and *cly1.c*, with respective mutations at the 8th and 14th positions (Nair et al. 2010) of the orthologous barley gene *Cly1* (Fig. II-3). In contrast to the two barley *cly1* alleles each carrying a synonymous SNP, the wheat mutant alleles identified here had non-synonymous SNPs. The translation products of *AP2-A1* and *AP2-D1* would have the Ala residue replaced with Val, while that of *AP2-D2* would have it replaced with Thr. Sequence comparison of PCR-amplified genomic DNA encompassing the coding region (ca. 2.8 kbp) confirmed that all three mutant alleles had no other nucleotide changes from the respective wild-type alleles.

Phenotypic assessment of mutants

Lines homozygous for the three point mutations grew comparably to the wild type in the field. At anthesis, all mutants flowered with a fairly normal exposure of anthers (Fig. II-4a). Lodicules of all mutants swelled at anthesis (Fig. II-4b), but their size differed significantly from those of the wild type (Fig. II-5, Table II-2). Most notably, lodicule depth was significantly reduced in all three mutants, being reduced most in *AP2-D2* (Fig. II-5c). Length and width showed a similar tendency in *AP2-D2*, though not in *AP2-A1* or *AP2-D1* (Fig. II-5 a, b).

AP2-D2 had much shorter spikes than the other mutants (see rachis length in Fig. II-6c; Table II-2) and showed a typical compact (dense) spike (Fig. II-4a). The shorter spike of *AP2-D2* was caused by a significant reduction in rachis internode length (Fig. II-6a; Table II-2), not in the number of rachis nodes (Fig. II-6b). The decrease in length was also found in *AP2-A1* and *AP2-D1* mutants, although to a lesser extent (Fig. II-6a).

All three null mutants deleting individual *AP2* homoeologs flowered at anthesis with lodicules swelled, 169B (*AP2-A*) and 248D (*AP2-D)* null mutants, exhibit a slight decrease in both lodicule length and width compared to the wild type. However, in 1131A (*AP2-A*) null mutant, there was no significant reduction observed. Additionally, there were no notable differences in rachis internode length when compared to the wild type. Nevertheless, the null mutants exhibited a distinctive speltoid (sparse) spike phenotype characterized by an elongated rachis, resembling a spear shape. No particular variations that would be specific to individual deletion mutations were found. Therefore, further trait analysis of them was considered inappropriate at this stage, because plants showing more general mutational signatures, e.g., poor growth, low fertility, morphological abnormality, etc. were segregated frequently in the progeny of null mutants. This is likely due to deleterious mutations other than a single deletion of target *AP2* homoeolog caused by gamma-irradiation, and thus the use of near-isogenic lines would be preferred for more precise trait evaluation of the null mutants.

Transcriptional profiling of mutant alleles

qPCR assay of immature spikes at the terminal spikelet stage and white anther stage revealed that the abundance of the *AP2-D* transcript was remarkably higher in *AP2-D2*, followed by *AP2-D1*, than in the wild type and *AP2-A1*, notably so in the younger spikes at the terminal spikelet stage (Fig. II-7). In contrast, the abundance of the *AP2-A* transcript was slightly higher in *AP2-A1* than in the others, especially at the white anther stage, although the differences were not as high as those of the *AP2-D* transcript.

Predicted interaction between miR172 and the target sites of mutant alleles

Relative to that in the wild type (−33.8 kcal/mol, mfe), the predicted interactions between miR172 and the target sites were reduced in all three mutants, more so in *AP2-D2* (−27.2 kcal/mol) than in *AP2-A1* and *AP2-D1* (−31.8 kcal/mol; Fig. II-8a). The result suggests that reduced interaction between mRNA and miR172 at the target site suppresses lodicule development and leads to a compact spike, as the notion was

supported by the similar results obtained in barley (Fig. II-8 b, c; described further in Discussion).

Discussion

Point mutations in the miR172 target site inhibit lodicule development

Lodicule swelling is the main factor that opens flowers at anthesis in wheat and other cereals by pushing apart the lemma and palea (Yoshida et al. 2007, Nair et al. 2010, Ning et al. 2013a, Ohmori et al. 2018). We found that lodicule size, particularly depth, was significantly reduced in all three mutants carrying a point mutation of wheat *AP2* homoeologs. However, none of the mutants flowered closed. This result indicates that the lodicules of all mutants could swell and expand, though not fully, sufficient for floret opening, despite a universal mechanical function of lodicule depth subject to SNPs in the miR172 target site in barley and wheat. The greatest reduction in lodicule depth was seen in the *AP2-D2* mutant, indicating that this mutation had larger functional effects than the other two mutations. We presume that the larger effect was caused by the reduced interaction between miR172 and the target mRNA sites of the mutants, described next.

Decreased interaction of miR172-mediated mRNA cleavage reduces lodicule size

Base pairing between miRNA and its target mRNA is crucial for mRNA cleavage (Huntzinger and Izaurralde 2011). Differences in miR172-guided cleavage of *Cly1* transcripts alter lodicule development and the consequent occurrence of cleistogamy (Nair et al. 2010). Importantly, similar mutations replace a strong G:C pair in the wild type with a G:U wobble pair in *AP2-A1* and *AP2-D1* and an A:C mismatch in *AP2-D2* (Varani and McClain 2000, Rehmsmeier et al. 2004) in the miR172 interactions, which could maintain weak interactions. The interaction in miR172 is much more reduced in *AP2-D2* than in *AP2-A1* and *AP2-D1*. The differences in interactions with miR172 could also affect the amount of AP2 protein translated, which is necessary for suppressing the development of lodicules.

The pronounced effect of the *AP2-D2* allele on lodicule size can be attributed to its significantly lower interaction with miR172 at the target site. This reduces the likelihood of miR172-mediated mRNA cleavage, resulting in higher transcript levels than from the *AP2-A1*, *AP2-D1*, and wild-type alleles. The results of qPCR analysis support this, showing high *AP2-D2* transcript levels at both spike development stages (Fig. II-7). Moreover, all SNP mutants expressed the gene at both development stages, *AP2-D2* particularly so. A previous expression analysis revealed that, while the expression patterns of *Cly1.a* (AZ) and *cly1.b* (KNG) are similar from the awn primordium stage to

the yellow anther stage, the transcript abundance of KNG is higher (Nair et al. 2010). miR172a regulates the expression of *Cly1* by inhibiting its translation, and the level of Cly1 protein is reduced in AZ (Anwar et al. 2018). It can be inferred that the abundance of translated protein in *AP2-D2* was sufficient to inhibit the full expansion of lodicules, although the difference in amino acid change between *AP2-D2* and *AP2-A1*/*D1* might also contribute to the reduction in lodicule size.

Reduced interaction between miRNA and its target mRNA at the miR172 target site results in compact spike morphology

Barley's cleistogamy alleles (*cly1.b* and *cly1.c*) derive from natural *HvAP2* gene variants (Nair et al. 2010). Induced *Zeocriton* (*Zeo*) gene mutants had interesting mutations in *HvAP2*, with three different point mutations identified in the miR172 target site (Houston et al. 2013, Fig. II-8c). The *Zeo1* mutant showed a very compact spike morphology with a remarkable increase in spike density. The phenotype was caused by significantly reduced elongation of rachis internodes. This dense-spike phenotype was much more severe in *Zeo1* than in *Zeo2* (= *cly1.b*) and *Zeo3* (= *cly1.c*). The degree of interaction with miR172 was predicted to be reduced relative to that of the wild-type allele (*Cly1.a*, −35.2 kcal/mol) to a much greater extent in *Zeo1* alleles (−30.6 to −30.8 kcal/mol) than in *Zeo2/cly1.b* (−34.8 kcal/mol) or *Zeo3*/*cly1.c* (−32.6 kcal/mol; Fig. II-8 b, c). Therefore, its severity in *Zeo1* may be due to the greater reduction in the miR172 binding affinity. Our result of wheat *AP2* mRNA interaction with miR172 supports this, where *AP2-D2* had a lower interaction than *AP2-A1* and *AP2-D1* (Fig. II-8a), resulting in a dense-spike morphology. Higher transcript levels result in a compact spike and reduced plant height, as found in another wheat *AP2* gene, *Q* (Simons et al. 2006). The result shows that the effect of the SNP in the miR172 target site on the reduction of rachis internode length is common in barley and wheat. Furthermore, the *Zeo1* mutants flower cleistogamously and lack lodicule swelling at anthesis.

Concluding remarks

This study evaluated the potential for developing cleistogamous wheat by analyzing three novel mutant alleles of *AP2* homoeologs. Lodicule depth was inhibited in the *AP2-A1*, *AP2-D1*, and *AP2-D2* mutants, although cleistogamy was not induced as observed in barley mutants. Although the mechanism is not elucidated, chasmogamous phenotype is expressed in barley genotypes heterozygous for *cly1* (*Cly1.a/cly1.b* or *Cly1.a/cly1.c*)

(Wang et al. 2015). In analogy with this phenomenon, the two wild-type homoeologs may act to compensate the effect of one mutated homoeolog in hexaploid wheat. Consequently, it would be interesting to test the combination of two mutant homoeologs along with the null mutants to investigate dosage effects of *AP2* mutations for cleistogamy. Targeted mutagenesis of *AP2-B* homoeologs may also be needed to test the initial hypothesis that combining miRNA-site mutations from all three *AP2* homoeologs within a single plant would result in the production of cleistogamous wheat. In addition to flowering traits, pleiotropy of *AP2* mutations is of particular importance to investigate as it would potentially influence a wide range of agronomic traits as well as spike density. The necessity of trait evaluation under near-isogenic genetic background will be required for more precise evaluation of those quantitative traits. All these issues need to be addressed in the next step of this research.

Table II-1 Primer sequences used in this study

Category	Target gene	Primer name	Primer sequence (5'-3')	Primer name	Primer sequence (5'-3')
Gene-specific amplification	*AP2-A*	F-est1320	TGCACGGCTGGGGCAACGTC	L3721A19	CGGTGGTGGAGCTGGCAAG
(HRM and null mutant screening)	*AP2-B*	F-est1180	TCATGGGCAACGGTGATCC	L3801L18	GCGCTGGCTGCTCTCGAC
	AP2-D	F-est1320	TGCACGGCTGGGGCAACGTC	L3897D22	GGTGGAGCTGGTCTTGATGGTC
3' UTR for qPCR	*AP2-A*	A3718U19	AAGCTTGCCAGCTCCACCA	A3794L19	CCCATGCTCCTCCGTGATC
(Real-time PCR)	*AP2-B*	B3960U19	GAGCTGAACTGAAACTTGA	B4052L19	CCGCATTTACATGACTGCC
	AP2-D	D3897U20	GACCATCAAGACCAGCTCCA	D4007L18	TGCATGCATGGTTGTGGT
	Actin	DN182500F425	AAGTACAGTGTCTGGATTGGAGGG	DN182500R533	TCGCAACTTAGAAGCACTTCCG

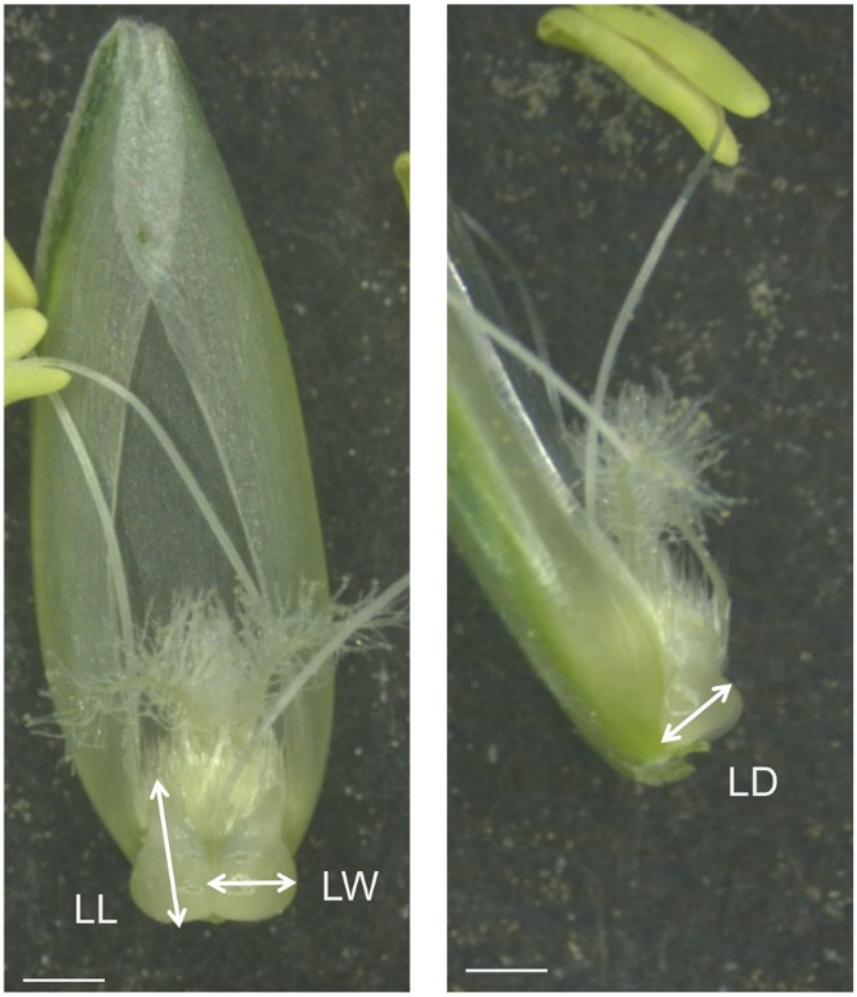

Fig. II-1 Measurement of lodicule length (LL), width (LW) and depth (LD). Bar: 1 mm.

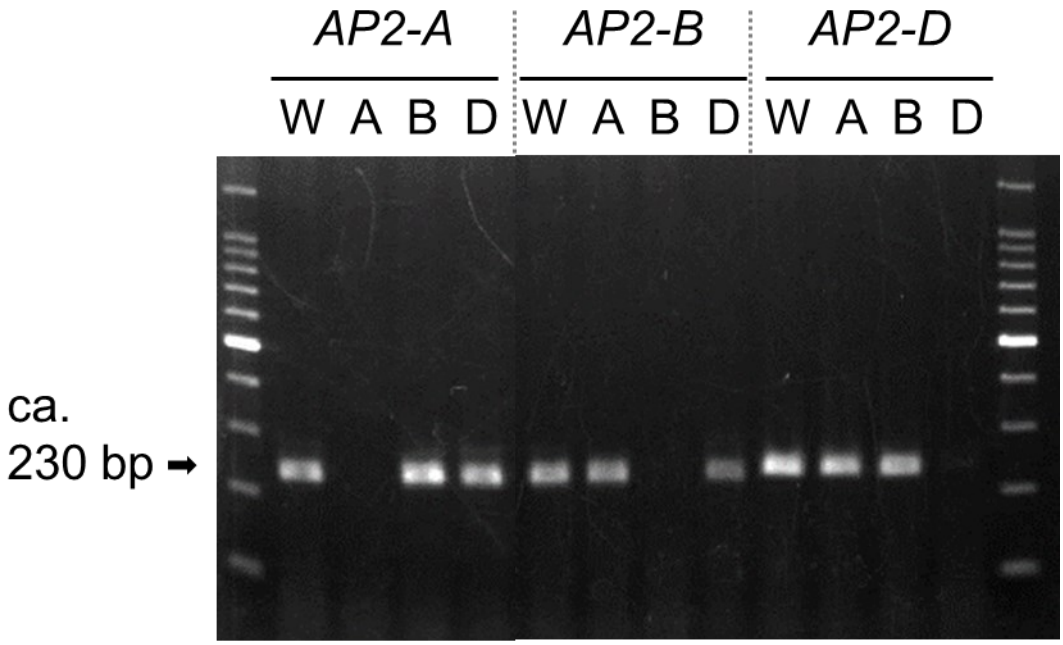

W : WT (‘Kitahonami’)

A : null mutant for *AP2-A* (1131A)

B : null mutant for *AP2-B* (169B)

D : null mutant for *AP2-D* (248D)

Fig. II-2 Gene-specific PCR showing the null (deletion) mutation in each *AP2* homoeolog. *AP2-A*, *AP2-B*, and *AP2-D* genes are deleted in the null mutants 1131A, 169B, and 248D, respectively. An arrow indicates the amplified product of target gene.

Fig. II-3 Sequence variation in the miR172 target sites of barley *HvAP2* and wheat *AP2* homoeologs. *AP2-A1*, *D1*, and *D2* are SNP mutant alleles identified among EMS-induced mutants of wild-type (WT) 'Kitahonami'. The miR172 sequence from wheat *miR172a* is indicated at the bottom.

a

b

Fig. II-4 Spikes and floral organs of wild-type (WT) and *AP2* mutants (*A1*, *D1*, *D2*). Spike at anthesis **(a)**, floret at anthesis **(b)** (upper panel) and side view of the lodicule (lower panel). Bar: 1 mm.

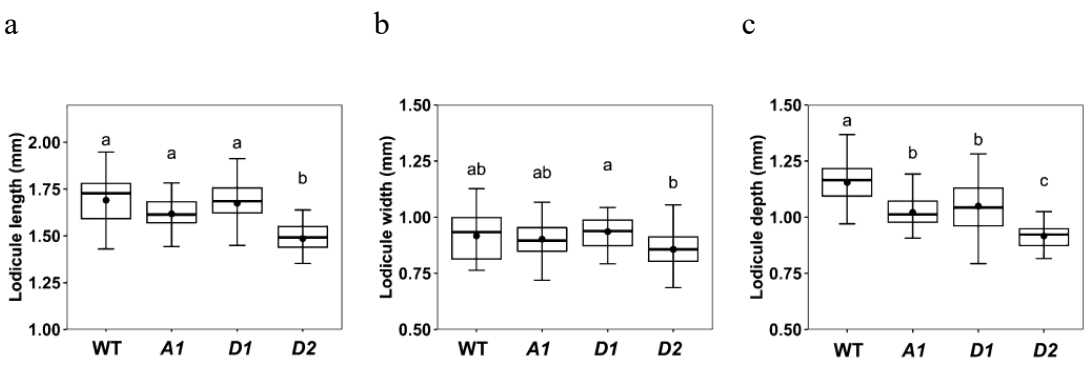

Fig. II-5 Comparison of lodicule size among wild-type (WT) and *AP2* mutants (*A1*, *D1*, *D2*). Length **(a)**, width **(b),** depth **(c)**. Thick horizontal lines indicate median (50% quartile), bullets indicate mean, and whiskers represent maximum and minimum values excluding outliers. Mean values with the same letter do not differ significantly ($P > 0.05$) by Tukey–Kramer HSD test.

Table II-2 Comparison of lodicule size and spike traits among the wild type and three *AP2* mutants (mean ± SE)

Genotype	Lodicule size				Spike traits			
	n	Length (mm)	Width (mm)	Depth (mm)	*n*	Rachis internode length (mm)	Rachis node number	Rachis length (cm)
WT	32	1.69 ± 0.02	0.90 ± 0.02	1.15 ± 0.02	30	4.15 ± 0.03	20.0 ± 0.17	8.30 ± 0.08
A1	32	1.62 ± 0.02	0.90 ± 0.01	1.02 ± 0.01	63	4.00 ± 0.05	19.7 ± 0.13	7.77 ± 0.17
D1	30	1.67 ± 0.02	0.94 ± 0.02	1.05 ± 0.02	69	4.07 ± 0.02	19.7 ± 0.09	7.98 ± 0.06
D2	26	1.49 ± 0.02	0.86 ± 0.02	0.92 ± 0.01	75	2.91 ± 0.02	19.5 ± 0.11	5.69 ± 0.06
ANOVA		***	*	***		***	n.s.	***

*, *** and n.s.: significant at 5%, 0.1% and not significant at 5% levels, respectively.
n: number of lodicules and spikes used.

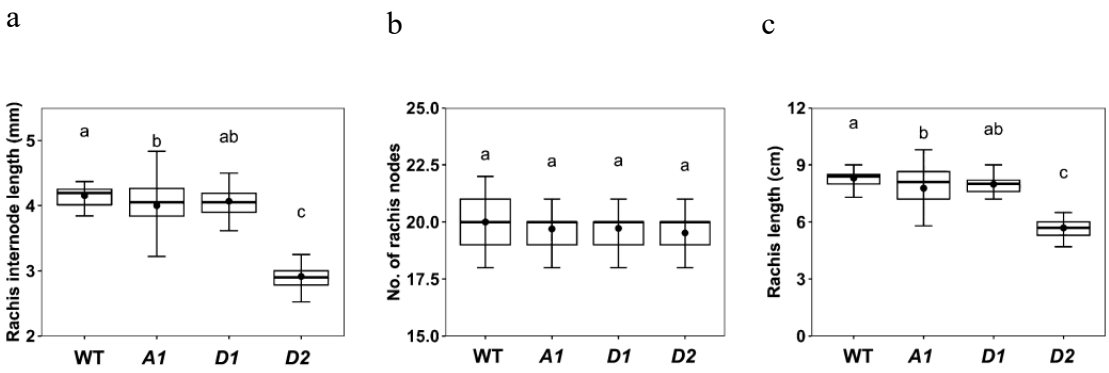

Fig. II-6 Comparison of spike rachis traits among wild-type (WT) and *AP2* mutants (*A1*, *D1*, *D2*). Rachis internode length **(a)**, number of rachis nodes **(b)**, rachis length **(c)**. Thick horizontal lines indicate median (50% quartile), bullets indicate mean, and whiskers represent maximum and minimum values excluding outliers. Mean values with the same letter do not differ significantly ($P > 0.05$) by Tukey–Kramer HSD test.

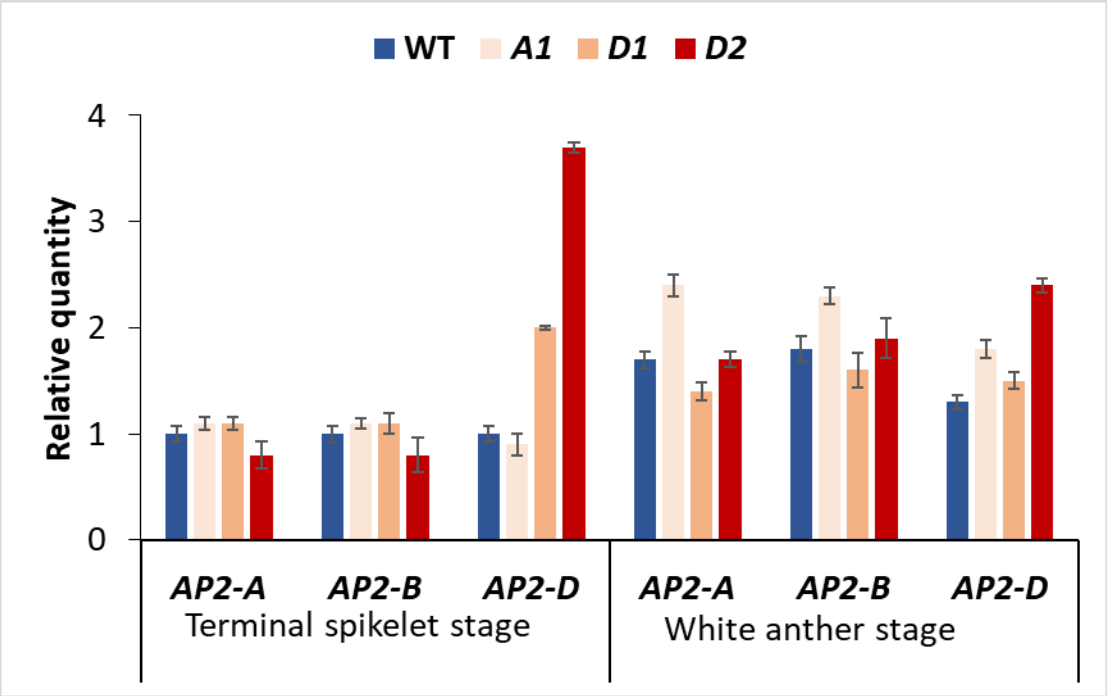

Fig. II-7 Transcript abundance of *AP2* homoeologs (*AP2-A*, *-B*, *-D*) in immature spikes at terminal spikelet and white anther stages by qPCR assay. Transcript abundances were normalized against that of *actin* and that of the WT at the terminal spikelet stage.

a b c

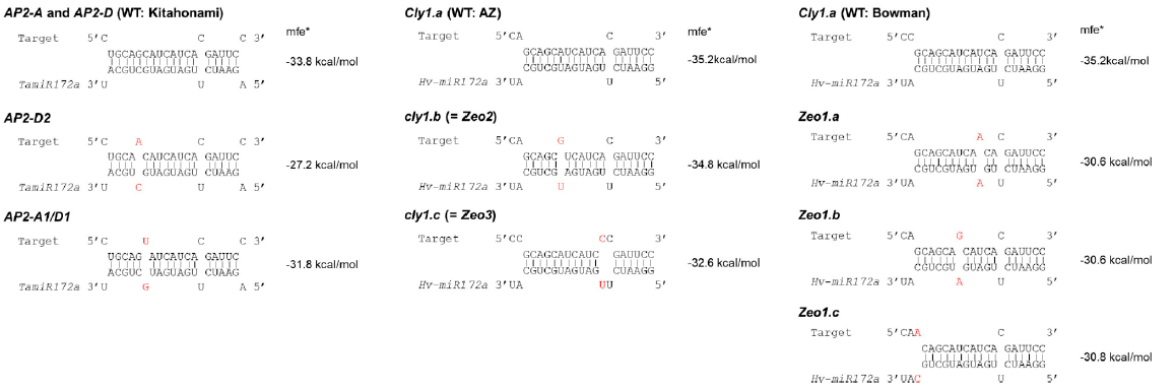

Fig. II-8 Predicted interactions between mRNA and miR172. Wheat *AP2* homoeologs **(a)** (this study), barley *cly1* **(b)** (Nair et al. 2010), barley *Zeo1* **(c)** (Houston et al. 2013). *mfe: minimum free energy (Rehmsmeier et al. 2004).

Chapter III

Accumulation of mutations in the *AP2* homoeologs causes suppression of anther extrusion with altered spike and culm development in hexaploid wheat

Introduction

Cleistogamy is the fertilization of closed flowers and is adapted to ensure reproduction under unfavorable conditions. Minimizing the gene flow in open-field cultivation is useful for practical breeding applications, particularly for genetically modified (GM) crops (Daniell 2002, Ni et al. 2014, Lombardo et al. 2016, Ohmori et al. 2012). Cleistogamy reduces the risk of fungal infection of the floret at anthesis, which is important for disease control, especially of Fusarium head blight (FHB) in Triticeae (Kubo et al. 2010, 2013 Yoshida et al. 2005, 2007). Cleistogamous barley cultivars (*H. vulgare*) are more resistant to Fusarium infection than wild-type chasmogamous (open-flowering) cultivars (Yoshida et al. 2007). Because of its practical importance, genetic analyses of cleistogamy in barley have shown that it is determined by a recessive gene at the *Cleistogamy 1* (*cly1*) locus on chromosome 2H (Turuspekov et al. 2004, 2005). Molecular studies have also led to the cloning of the *Cly1* gene, which encodes a barley ortholog of the *Arabidopsis* Apetala2 (AP2) transcription factor (Nair et al. 2010). The wild-type *Cly1* allele (*Cly1*.a) contains an miR172 target site, whereas the natural variant *cly1* allele (*cly1.b* or *cly1*.c) contains a single nucleotide polymorphism (SNP) within the miR172 target site. A point mutation in the cleistogamous *cly1* allele inhibits the binding of miR172 to the target site of the mRNA, resulting in the production of the Cly1 protein (HvAP2). This protein negatively regulates the development of lodicules through which full swelling allows florets to open, thereby keeping them closed during anthesis (Anwar et al. 2018).

Bread wheat (*T. aestivum*) is a hexaploid consisting of three subgenomes (A, B and D), each containing seven chromosomes. Three wheat orthologs of barley *Cly1* (*HvAP2*), including *AP2-A* (gene ID: 123190780), *AP2-B* (gene ID: 123047120) and

AP2-D (gene ID: 123054929) (these are also collectively referred to as *AP2L2*, Debernardi et al. 2020), show structures and transcriptional patterns similar to those of barley *Cly1* (Ning et al. 2013a). These genes contain a conserved miR172 target site. However, no natural sequence variation within the site has been detected in the three *AP2* homoeologs despite an extensive sequence survey of diverse wheat germplasms and wild relatives (Ning et al. 2013b). Complete cleistogamy, comparable to that of barley, has not yet been demonstrated in wheat cultivars. In a previous study, we induced and isolated novel mutations within the miR172 target site in wheat *AP2* homoeologs using ethyl methanesulfonate (EMS) mutagenesis and high-resolution melt (HRM) analysis (Chapter II). Three independent point mutations were identified at the miR172 target sites of *AP2-A* and *AP2-D* genes, although no miR172 target site mutations were detected in *AP2-B*. These point mutations were different from those present in the barley *cly1* alleles. The two mutant alleles, *AP2-A1* and *AP2-D1*, shared the same SNP in terms of position and nucleotide substitution, whereas the other mutant allele, *AP2-D2*, had a distinct SNP (Fig. III-1). These mutants showed reduced lodicule size, although they showed visually normal open flowering during anthesis. In addition, the *AP2-D2* mutant had a reduced rachis internode length, resulting in a compact spike.

Our initial hypothesis that the mechanism of barley *cly1* could be applied to wheat cleistogamy suggested a possible strategy for engineering cleistogamous wheat by accumulating point mutations at the miR172 target site of all three *AP2* homoeologs in a single plant (Ning et al. 2013a). Here, we investigated whether the accumulation of mutant *AP2* alleles suppressed open flowering in wheat without a point mutation in *AP2-B*. Near-isogenic lines (NILs) were developed from single *AP2* mutants and crossed to obtain double mutants. The anther extrusion rate was used to assess the level of flowering, and its correlation with lodicule size was investigated. We investigated the pleiotropy of miR172 target site mutations during spike and culm development.

Materials and methods

Plant materials

The NILs of three single *AP2* mutants previously induced by EMS mutagenesis (Chapter II) were generated (Fig. III-2 a-c). The original mutants carrying *AP2-A1*, *D1* and *D2* alleles (selfed progeny of 038E, 514E and 190E, respectively) were crossed with the parental cultivar 'Kitahonami.' F_1 plants were backcrossed three times with 'Kitahonami' as the recurrent parent, and PCR-based genotyping was performed as described below. Three BC_3F_2 populations were obtained, each segregating the *AP2-A1*, *D1* and *D2* alleles (designated 038BC_3F_2, 514BC_3F_2, and 190BC_3F_2, respectively). Homozygous BC_3F_2 plants for each mutant allele were then selfed to produce three single mutants, and BC_3F_2 to BC_3F_4 plants were used for trait analysis. Two double mutants were obtained by crossing the NILs of two single mutants, as shown in Fig. III-3 a, b. The F_2 and F_3 progeny of the BC_2F_1×BC_2F_1 plants and the F_3 progeny of the BC_3F_1×BC_3F_1 plants were used to select double mutants homozygous for *AP2-A1* and *AP2-D1* (*AP2-A1/AP2-D1*), and *AP2-A1* and *AP2-D2* (*AP2-A1/AP2-D2*).

Three null mutants lacking each *AP2* homoeolog that were previously induced by gamma irradiation (Chapter II) were used to generate the NIL of each null mutant (Fig. III-4 a-c). Single-null mutants were obtained from the BC_3F_2 progeny (designated *ap2-A*, *ap2-B* and *ap2-D*), and the BC_3F_4 progeny plants were used for trait analysis. The BC_3F_3 progeny of the single-null mutants were crossed to generate double-null mutants. Two double-null mutants (designated *ap2-A/ap2-B* and *ap2-A/ap2-D*) were obtained, although another possible double mutant (*ap2-B/ap2-D*) was not obtained from any of the F_2 progenies of the *ap2-B*×*ap2-D* cross. Finally, the double mutant *AP2-A1/AP2-D2* was crossed with the null mutant *ap2-B* to generate the mutant genotype *AP2-A1/ap2-B/AP2-D2*. Plants homozygous for each of the three alleles were screened in the F_2 progeny and the F_3 progeny plants were used for trait and expression analyses.

The plants used for phenotypic evaluation were grown in a field at Mie University. Seeds were sown in mid-November, and the seedlings were maintained in a cell tray in a greenhouse until they were transplanted into the field

in early to mid-December. Plants were spaced 10 cm apart in two rows that were 30 cm apart. Each row was separated from the adjacent rows by 50 cm. Most plants begin to flower in late April or early May. The survey was conducted over three years in the spring of 2020–2022.

Genotyping

Genomic DNA extracted from young leaves was used for PCR to determine *AP2-A*, *AP2-D* and null *ap2-A, ap2-B and ap2-D* genotypes in the cross-progeny. The primers and PCR conditions used for *AP2* allele-specific amplification are listed in Table III-1. The presence or absence of the resulting amplicons was visualized by electrophoresis on a 3% agarose gel stained with ethidium bromide (Fig. III-5).

Calculation of anther extrusion rate

The anther extrusion rate from the florets was calculated as follows: The number of anthers remaining in each floret (0–3) was first counted in the first and second florets of a spike collected 7–10 d after anthesis, when the kernels were approximately half or two-thirds of their mature size, excluding the top two and bottom four spikelets (including the incomplete ones). The total number of extruded anthers per spike was then calculated and divided by the number of florets examined. The average number of extruded anthers per spike was calculated and expressed as percentage. Seed fertility (% seed set) was also assessed per spike, using the same spikes as those examined for the anther extrusion rate. About 10–20 spikes (one spike per plant) were used for each genotype.

Measurement of lodicule and other floral organ size

Lodicule size was measured as described in Chapter II. Briefly, the length, width and depth of each lodicule were measured in the first and second florets at anthesis. About 30–90 lodicules were measured for each genotype. The lengths and widths of the palea and anthers were measured in the same florets. Because the size of the lodicule relative to the floret is critical for floret opening, the relative lodicule size was defined as the length, width, and depth of the lodicule divided by the palea width of the same floret.

Measurement of spike, culm and other agronomic traits

Rachis internode length was measured as described in Chapter II. The mean rachis internode length was calculated as an indicator of spike density by dividing the rachis length by the number of rachis nodes per spike. Approximately 10–20 spikes were used for each genotype. The present analysis compared rachis length at three positions (basal, central and apical), equally divided based on the rachis node number, to examine

positional differences in rachis internode elongation (using plants evaluated for agronomic traits, as described next). In addition, the lengths of the immature spikes were compared as spike development progressed from the floret primordia stage to the yellow anther stage using 'Kitahonami' and a single *AP2-D2* mutant. The following spike development stages were determined based on Kirby and Appleyard (1981), which also correspond to the wheat growth stage referred to as the GS number (decimal code defined by Zadoks et al. 1974): Floret primordium stage (GS22); Terminal spikelet stage (GS29); White anther stage (GS32); Green anther stage (GS35-45); Yellow anther stage (GS47-59).

Culm internode length and other agronomic traits were evaluated in 2-year field trials. A set of six genotypes ('Kitahonami' (WT), three single and two double mutants) was grown in three replicates with slight modifications to our conventional planting pattern, as described in ***Plant materials***. Plants were spaced 10 cm apart in four rows and 15 cm apart, with the five mutant genotypes tested and the WT, in the two middle rows, and only the WT as a border plant in the two outer rows. Five plants per replicate were selected from each genotype for subsequent analysis.

A dried mature plant collected from the field with the roots cut off was used to measure the dry plant weight, and the longest tiller was selected to measure the culm length (from the base of the tiller to the neck of the spike). Culm internode length was generally measured on five to six internodes, with the length of the uppermost internode (just below the spike) designated as internode length 1 (IL1) and subsequent internode lengths numbered accordingly (IL2 to IL6). After counting the effective tillers, spikes were harvested from the five longest tillers per plant to measure several spike characteristics (spike (rachis) length and weight, number of rachis nodes, and fertile spikelets). Finally, all grains were collected from each spike. The number of grains per spike was counted and used to calculate the average number of grains per spikelet, based on the number of fertile spikelets per spike. The total grain weight per spike was measured. Grain size (length, width, and depth) was measured using a caliper gauge with 15 grains per genotype (five grains per replicate).

All measured data were analyzed using one-way ANOVA followed by Tukey's honestly significant difference (HSD) test for multiple comparisons ($P < 0.05$) or Student's t-test for two-sample comparisons.

Expression analysis

Total RNA was extracted from immature spikes at the terminal spikelet or white anther stage of 'Kitahonami' (WT) and mutant genotypes (*AP2-A1*, *AP2-D1*, *AP2-D2*, *AP2-A1/AP2-D2* and *AP2-A1/ap2-B/AP2-D2*). Total RNA was also extracted from several floral organs (lodicule, anther, pistil, lemma, palea and glume) and plant tissues (rachis, culm internode, culm node and leaf) collected from the WT and *AP2-D2* mutant one day before anthesis. The procedures for RNA extraction, cDNA synthesis, and qPCR assays were as described in Chapter II.

RESULTS

Anther extrusion

Previous investigations of the original mutants showed that all three exhibited open flowering with normal anther exposure during anthesis (Chapter II). Similarly, all mutant homozygotes (M genotype) of the three BC_3F_2 NILs (Fig. III-2) flowered upon anther exposure (Fig. III-6a). Both the wild-type homozygotes (W genotype) and heterozygotes (H genotype) in the three NILs also flowered. However, no clear differences in the degree of flower opening were detected among the three genotypes by visual assessment. Therefore, the anther extrusion rate was examined as an index of the flowering phenotype. The comparison between the three genotypes (W, H and M) in each BC_3F_2 showed that, specifically in *AP2-D2*, the level of anther extrusion was significantly reduced in the M genotype than in the H and W genotypes (Fig. III-7a). The anther extrusion rate was 53.5±2.6% (of 100%) in M, 67.7±1.6% in H and 80.2±1.1% in W (Table III-2). This indicated that the level of anther extrusion in the *AP2-D2* mutant was approximately two-thirds of that in the wild type. The *AP2-D2* allele had an additive effect in reducing anther extrusion based on the mean value of H. In contrast, no significant differences in anther extrusion were detected among the three genotypes of either *AP2-A1* or *AP2-D1*.

Next, two double mutants (*AP2-A1/AP2-D1* and *AP2-A1/AP2-D2*) with three single mutants (*AP2-A1*, *AP2-D1* and *AP2-D2*), homozygous for the respective mutant allele(s) and selected from NILs, were used for genotypic comparison with the wild type 'Kitahonami' (WT). The three single mutants did not appear to flower differently from the WT under visual inspection in the field, as observed in the original mutants (Chapter II). However, one of the double mutants, *AP2-A1/AP2-D2*, appeared to differ in terms of flowering suppression with poor anther exposure during anthesis, whereas another double mutant, *AP2-A1/AP2-D1*, did not show any particular features in this respect (Fig. III-6a). Genotypic comparison of anther extrusion rates over a two-year period revealed that the double mutant *AP2-A1/AP2-D2* had the lowest value (40.3% and 31.7% in 2020 and 2021, respectively) compared to the WT (85.7% and 77.7%, respectively) (Fig. III-7b, Table III-3). The single mutant *AP2-D2* also showed a significant decrease in anther extrusion rate (53.5% and 51.0%), although this was not visually clear in the field. In the other three mutants, the anther extrusion rate was not significantly different from that of the WT, except in 2020 when only the *AP2-A1* mutant showed a significant decrease.

Most importantly, the double mutant *AP2-A1/AP2-D2* showed significantly lower anther extrusion than did the single mutant *AP2-D2*, indicating that the strong effect of the *AP2-D2* allele could be further enhanced by the accumulation of another allele, *AP2-A1*, which has a milder effect on its own.

Three single-null mutants flowered with normal anther exposure at anthesis, although the anther extrusion rate was significantly reduced in both double-null mutants, especially in *ap2-A/ap2-B* (Fig. III-8a, Table III-4). The mutant genotype *AP2-A1/ap2-B/AP2-D2*, consisting of two mutant alleles, *AP2-A* and *AP2-D2*, with the deletion of the *AP2-B* homoeolog, showed a remarkable reduction in the anther extrusion rate, but this was not significantly different from that of the double mutant, *AP2-A1/AP2-D2* (Fig. III-9a, Table III-5).

Lodicule swelling

Focusing on the relative lodicule size, which corresponds to the size relative to palea width, there was a consistent reduction in the *AP2-D2* homozygote (M) compared to the wild type (W) in the BC_3F_2 NIL (Fig. III-10 d-f, 11b, Table III-2). Both double mutants exhibited swollen lodicules during anthesis (Fig. III-6b). A detailed examination of their size revealed that the double mutant *AP2-A1/AP2-D2* showed a consistent reduction in lodicule size in terms of length, width and depth compared with the WT, with mean values mostly significantly different between the two genotypes (Fig. III-7 d-f, Table III-3). Among the three single mutant alleles, the *AP2-D2* allele had the most pronounced effect on lodicule size reduction, whereas neither the *AP2-A1* nor *AP2-D1* alleles had a significant effect. The double mutant *AP2-A1/AP2-D2* consistently showed lower lodicule length and depth than the single mutant *AP2-D2*, although only lodicule length in 2020 and lodicule depth in 2021 differed significantly (Fig. III-7 d-f), which was also supported by the relative lodicule size (Fig. III-12 a-c). The results obtained here support the accumulation effect of the *AP2-A1* allele, as described for anther extrusion, which was further confirmed by direct comparison of lodicule depth and anther extrusion using single-plant data between *AP2-D2* and *AP2-A1/D2* mutants (Fig. III-7c). Furthermore, the correlation between lodicule width and depth indicated that the double mutant *AP2-A1/AP2-D2* shows a greater reduction in lodicule width and depth than the *AP2-D2* mutant (Fig. III-12d).

The lodicule sizes of all five null mutants (three single- and two double-null mutants) were generally similar to those of the WT, except for some genotypic variation in lodicule length (Fig. III-8 b-d, Table III-4). However, there was no correlation between

lodicule depth and anther extrusion rate (Fig. III-8 a, d). The retention of more anthers in both double-null mutants may be due to the mutational influence of the gamma irradiation-deleted chromosomal regions, which, although unidentified, were not compensated for by backcrossing. The *AP2-A1/ap2-B/AP2-D2* mutant had reduced lodicule size, similar to the double mutant *AP2-A1/AP2-D2*, in which only the lodicule width showed a significant difference (Fig. III-9 b-d, Table III-5).

Spike compactness

The *AP2-D2* mutant was characterized by a compact spike (Fig. III-6a). A significant reduction in rachis internode length, which is the cause of the compact spike (Chapter II), was observed not only in the M genotype, but also in the H genotype, compared to that in the W genotype (Fig. III-13, Table III-2). Importantly, the pattern of reduction from W to M was consistent between rachis internode length and anther extrusion rate (Fig. III-7a), clearly indicating an additive effect of the *AP2-D2* allele on both traits. Although much smaller than *AP2-D2*, both the *AP2-A1* and *AP2-D1* alleles appeared to have an additive effect on reducing the rachis internode length, as shown in their respective BC_3F_2 NILs (Fig. III-13a). A comparison of six genotypes, including two double mutants and the WT, clearly showed that both the *AP2-D2* and *AP2-A1/AP2-D2* mutants had significantly shorter and more compact spikes (rachis length in Fig. III-13c), which was confirmed by a significant reduction in the length of the rachis internode (Fig. III-13b), while maintaining the number of rachis nodes (Fig. III-13d, Table III-3). Two single mutants, *AP2-A1* and *AP2-D1*, also showed a reduction in rachis internode length, but to a lesser extent (Fig. III-13b). Interestingly, the double mutant *AP2-A1/AP2-D1* showed a more significant reduction in rachis internode length than the single mutants *AP2-A1* or *AP2-D1*, indicating an accumulation effect of the two weaker alleles. In contrast, both the *AP2-D2* and *AP2-A1/AP2-D2* mutants showed the same degree of reduction in rachis internode length (Fig. III- 13b), resulting in the same compact spike length (Fig. III-13c). This suggests that the *AP2-D2* allele may have a remarkably strong effect on reducing rachis internode length.

Null mutants showed elongation of the rachis internode, while maintaining a constant spike (rachis) length (Fig. III-8 e, f, Table III-4). The degree of elongation was more significant in the two double-null mutants and one single *ap2-D* mutant than in the two single-null mutants *ap2-A* and *ap2-B*. However, there were no significant differences between them. These results are consistent with the null mutation, which abolished the function of AP2. The *AP2-A1/ap2-B/AP2-D2* mutant had significantly reduced rachis

internode length, but this was not significantly different from that of the *AP2-A1/AP2-D2* double mutant (Fig. III-9e). Overall, the wild-type *AP2-B* homoeolog had little effect on any phenotype compared to the *AP2-A1/AP2-D2* double mutant.

We examined the positional differences in rachis elongation. At three positions (apical, central and basal) on the spike, equally divided based on the number of rachis nodes (Fig. III-13e), the rachis length of both the *AP2-D2* and *AP2-A1/AP2-D2* mutants showed the greatest reduction at the apical position, followed by the central and basal positions on the spike, compared to the WT and other mutants (Fig. III-13f, 14a, Table III-6). This indicated that the elongation of the rachis internode in the two *AP2-D2* carrying mutants was suppressed more at the apical position than at the central and basal positions. Consequently, they had a marked difference in the spike architecture compared to the WT, with the grain density gradually increasing from the bottom to the top of the spike. Finally, we compared the spike length with the progression of the spike developmental stage between the single *AP2-D2* mutant and the WT. The significant difference in spike length appeared at the early immature stage (terminal spikelet stage) and gradually became more pronounced towards the later mature stage (yellow anther stage) (Fig. III-13g).

Other agronomic traits

Single and double mutants carrying the *AP2-D2* allele appeared to have reduced culm lengths compared with the WT and other mutants (Fig. III-15a). Both the *AP2-D2* and *AP2-A1/AP2-D2* mutants had significantly reduced culm lengths compared to the other mutants, which was consistent over two years (Fig. III-15c, Table III-7). Closer examination of the internodes revealed a significant reduction in the length of the uppermost internode (internode length 1; IL1) in both mutants (Fig. III-15b, d, Table III-7). The length of IL1 was not significantly different between the two mutants. These results consistently demonstrate that the reduced plant height in both mutants was primarily caused by a significant reduction in the uppermost internode length when combined with other internode lengths (Fig. III-15e, 14b).

We examined yield-related traits, including biomass weight, number of tillers, spike weight, effective number of spikelets per spike, grain weight per spike, and total number of grains per spike, over two years (2021–2022) (Fig. III-16 a-f). These quantitative traits showed year-to-year variability between the mutant and WT genotypes, with few agronomically positive traits consistently observed from any mutant. No

significant differences in grain size and shape were consistently observed over the two years (Fig. III-16 a-c).

Transcriptional profiling of the mutant alleles

The expression levels of the *AP2-D* homoeolog were examined in various floral organs and plant tissues and compared between the mutant *AP2-D2* and the WT alleles (Fig. III-18a). Among the floral organs, transcript levels of the mutant allele were higher than those of the WT in the lodicule, pistil and anther, whereas they were lower in the glume and lemma. The exceptionally high expression in the anther was interesting because anther size (length, width, and length/width) was particularly different in the *AP2-D2* mutant (Fig. III-11d, f, 12f, Table III-2, 3). This mutant had the largest length but the smallest width, resulting in the slimmest shape, represented by the largest length/width value among all genotypes. However, it was only significantly different from that in the WT. In other plant tissues, the culm internode (the uppermost internode) and the rachis showed marked differences in transcript levels between the mutant and WT alleles. In contrast, the culm nodes showed a smaller difference, while the leaves showed the opposite pattern (Fig. III-18a). These results supported the observed reduction in culm and rachis internodes in mutants carrying the *AP2-D2* allele.

qPCR was used to analyze the gene expression of the mutant alleles in immature spikes at the terminal spikelet and white anther stages using single and double mutants. In particular, higher transcript abundance of the mutant *AP2-D2* allele than that of the WT allele was consistently observed at both spike developmental stages (Fig. III-19). In the double mutant *AP2-A1/AP2-D2*, the *AP2-D2* allele showed higher transcript abundance than the WT allele at both stages, whereas the transcript level of the *AP2-A1* allele relative to that of the WT allele was not consistent between the two stages (Fig. III-18b). The mutant genotype *AP2-A1/ap2-B/AP2-D2*, showed higher transcript abundance of both the *AP2-A1* and *AP2-D2* alleles than the double mutant, especially at the white anther stage. However, this was not observed at the terminal spikelet stage (Fig. III-18b).

DISCUSSION

Accumulation of mutations in the miR172 target site of AP2 homoeologs reduces anther extrusion to partially suppress open flowering

Grasses commonly induce anther emergence during flowering via filament elongation. Anthers are often released early in the morning, when plant cells are well hydrated (Cheignon et al. 1973, Heslop-Harrison and Heslop-Harrison 1996, van Doorn and van Meeteren 2003, Zajączkowska et al. 2021). The anthers are extruded when the lodicules swell, resulting in floret opening. The present analysis showed that anther extrusion was suppressed in the *AP2-D2* mutant compared to that in the wild type and the other two single mutants by examining the rate of anther extrusion. The degree of reduction was dose-dependent for the mutant allele. This result is consistent with the finding that a point mutation in the *AP2-D2* allele has a greater effect on miR172 activity than other mutant alleles, as suggested by the low-energy interaction between *AP2-D2* mRNA and miR172 (Chapter II). This study further showed that the double mutant, *AP2-A1/AP2-D2*, had a significantly lower anther extrusion rate than the single *AP2-D2* mutant, demonstrating that accumulation of the *AP2-A1* allele had a significant cumulative effect on anther retention. These changes in anther extrusion were largely consistent with changes in lodicule size.

Cleistogamous barley cultivars carrying a natural variant allele, *cly1.b* or *cly1.c*, are characterized by failure of lodicule development with virtually no swelling, resulting in complete absence of anther extrusion (Honda et al. 2005, Nair et al. 2010, Wang et al. 2013, 2021). In marked contrast, the double mutant *AP2-A1/AP2-D2* with highly suppressed anther extrusion, had swollen, although not complete, lodicules with apparent vascular tissue. Thus, accumulation of the two *AP2* homoeologs was insufficient to achieve cleistogamy in wheat. Partial suppression of lodicule swelling has been observed in incomplete cleistogamy, as reported for a barley cultivar (SV235) carrying the *cly1.b2* allele (Nair et al. 2010, Wang et al. 2015). This epiallele variant had a coding sequence identical to that of *cly1.b*, but repressed transcription. It exhibited cleistogamy in the field, but florets opened on excised tillers treated with 2,4-D. The lodicules were partially atrophied under natural conditions to keep the florets closed but could expand sufficiently to open the floret upon application of exogenous auxin, resulting in cleistogamy failure. In this case, the reduction in lodicular vascularization was visualized using microscopy through the transparent area of the lodicules. However, in the case of the *AP2-A1/AP2-*

D2 mutant, there was no clear reduction in the transparent area, even after 2,4-D treatment (data not shown).

The hexaploid wheat accessions 'U24' and 'Corringin' were once reported to be cleistogamous wheat (Ueno and Itoh 1997). Observations of the flowering characteristics in the field indicated that neither exhibited true cleistogamy (data not shown). 'Corringin' was chasmogamous with a fair degree of anther extrusion, whereas 'U24' showed very few extruded anthers but floret opening, although not as obvious, on careful observation at anthesis. Interestingly, 'U24' had fully swollen lodicules with normal miR172 target site sequences in all three *AP2* homoeologs, but filament elongation was significantly suppressed at anthesis (data not shown), as also suggested by Kubo et al. (2010), suggesting unknown genetic factors controlling anther extrusion other than the *AP2* gene. Recently, Tang et al. (2019) reported an induced wheat mutant, *ZK001*, that exhibited cleistogamous flowering with smaller lodicules that did not absorb water compared to the wild type (YM18). They showed that the variation in lodicule size was likely due to reduced calcium and potassium concentrations in *ZK001*, which affected osmotic adjustments and signaling associated with water uptake and lodicule enlargement. *ZK001* also contained low levels of gibberellic acid (GA) and high levels of jasmonic acid (JA) in its lodicules, which may have contributed to its smaller size. Despite the lack of sequence information, it is unlikely that the mutations responsible for the cleistogamy of *ZK001* were induced in *AP2* homoeologs, as multiple miR172 target-site mutations in different *AP2* homoeologs would not occur simultaneously by single static magnetic field mutagenesis. However, it would be interesting to observe further progress in the genetic analysis of this mutant.

Mutations in miR172 target site have pleiotropic effects on spike and culm development

Mutations in the miR172 target site have pleiotropic effects on wheat spikes and plant architecture, significantly reducing the lengths of the rachis and culm internodes. A positional effect was primarily observed in the upper parts of both tissues. However, an accumulation effect in the double mutant *AP2-A1/AP2-D2* was not observed in either tissue, possibly because the sole effect of the *AP2-D2* allele may be strong enough to reach the reduction limit. In contrast, a dose-dependent decrease in the rachis internode elongation was observed for each *AP2* mutant allele. The data also showed that even the weaker alleles *AP2-A1* and *AP2-D1* had a significant additive effect on rachis internode reduction, suggesting that this is a good marker for evaluating the effects of mutations.

Expression analysis in different tissues supported these findings, as the transcript of the *AP2-D2* allele was detected more abundantly in the rachis, culm and immature spikes than in the wild-type allele. Point mutations in the miR172 target site of the barley *HvAP2* gene have also been reported to result in compact spikes, with an allelic series of induced *ZEOCRITON1* (*Zeo1*) mutants showing a greater reduction in rachis internodes than milder *Zeo2* (*cly1.b*) and *Zeo3* (*cly1.c*) mutants (Houston et al. 2013). One of the *Zeo1* alleles, *Zeo1.b*, shows reduced plant height, specifically a reduction in the final 'peduncle' internode, corresponding to the uppermost internode, by reducing proliferation and expansion and causing precocious maturation of the internode (Patil et al. 2019). The present results for wheat agree with these findings for the barley *AP2* orthologs.

The wheat *AP2* gene family has been differentiated into three groups, and the group containing the miR172 target sequence was classified as the *euAP2* group (Zhao et al. 2019). Gene homologs of the *euAP2* group were found in four different homoeologous groups 1, 2, 5 and 7, named *AP2L1*, *AP2L2*, *AP2L5* and *AP2L7*, respectively (Debernardi et al. 2020). The three *AP2* homoeologs analyzed in this study belong to *AP2L2*, and its related paralog *AP2L5* contains the well-known gene *Q* on chromosome 5A (Greenwood et al. 2017, Simons et al. 2006, Zhang et al. 2019, Zhang et al. 2022). The *Q* gene controls many agronomic traits such as plant height, threshability and glume tenacity (Zhang et al. 2022). A mutation in the miR172 target site of the *Q* gene has been shown to result in a dense (compact) spike phenotype and free threshing with increased transcript levels (Greenwood et al. 2017), which was also found in another *Q* mutant with a different point mutation at the miR172 target site (Xu et al. 2018) (Fig. III-20a). Greenwood et al. (2017) showed that the mutant allele has a dose-dependent effect on the spike phenotype, similar to the mutant *AP2-D2* allele in this study. However, this mutation did not reduce lodicule swelling, suggesting that the miR172 target site mutation in the *Q* gene alone is not involved in lodicule development. Using an artificial target mimicry (MIM) approach, Debernardi et al. (2017) showed that *MIM172* plants with reduced miR172 activity exhibited compact spikes with an allele-dose-dependent effect. Furthermore, high transcript levels were detected at the apical position, followed by the central and basal positions, which is consistent with a reduction in the rachis internode, with the highest level observed at the apical position, as observed in the *AP2-D2* mutant in this study. Point mutations in the miR172 target site of the *Q* gene have also been found to reduce culm length by increasing transcript levels (Greenwood et al.

2017, Xu et al. 2018, Zhang et al. 2019). These findings in the *Q* gene suggest partially redundant roles for *AP2L5* and *AP2L2* in spike and culm development.

Implications of current findings and future perspectives for the development of cleistogamous wheat

The accumulation of *AP2* homoeologs with mutations in the miR172 target site can significantly suppress anther extrusion. These findings are critical for achieving cleistogamy in hexaploid wheat. Suppression of anther extrusion was limited by the available mutations, and the mutant alleles were not sufficient to induce cleistogamy. The presence or absence of the wild-type *AP2-B* homoeolog had no significant effect on phenotype. The combination of different miR172 mutations, especially *AP2-B*, is of particular interest for testing the feasibility of cleistogamy. Debernardi et al. (2020) recently identified a novel point mutation in the miR172 target site of the *AP2-B* homoeolog (*AP2L-B2*) in a dwarf compact spike mutant induced in hexaploid wheat cv. 'Wedgetail,' which was first discovered for the *AP2-B* homoeolog. The mutant carrying this allele, *rAp2l-B2* (resistant *Ap2l-B2*), had smaller lodicules with a significantly reduced (30%) swollen area, although this did not lead to cleistogamy, together with a remarkably compact spike and shorter plant height. The *rAp2l-B2* allele has a point mutation from G to A at position 16 within the miR172 site, resulting in an Arg-to-Gln substitution in the encoded protein (Fig. III-20b), which differs from the point mutations in the three mutant alleles used in this study (Fig. III-1). Importantly, this mutant allele is expected to have a strong effect on miR172 activity, as it has a much lower interaction with miR172 (predicted from a minimum free energy (mfe) of -29.7 kcal/mol) than the wild-type *AP2-B* allele (mfe, -33.0 kcal/mol). The reduced level of interaction is comparable to that of the *AP2-D2* allele (mfe, -27.2 kcal/mol; Chapter II). Therefore, it is of particular interest to combine the *rAp2l-B2* allele with our two mutant alleles, *AP2-A1* and *AP2-D2*, and test the resulting triple mutant carrying all three mutant homoeologs for cleistogamy and the dosage effects of mutant allele combinations.

Recent studies on barley *HvAP2* have revealed its broad functions ranging from floral identity determination to flower organ development and tissue morphogenesis (Patil et al. 2019, Shoesmith et al. 2021). A series of recent studies on wheat *AP2-like* (*AP2L*) genes and miR172 have revealed further complex functions arising from the interactions between *AP2* homoeologs (*AP2L2* genes) and other *AP2L1* and *AP2L5* genes (Debernardi et al. 2020, 2022). Together with these findings, the present study shows that mutations in the miR172 target sites of *AP2* homoeologs have pleiotropic effects on

a variety of agronomically important traits, including compact spikes, reduced plant height, and possibly grain size and number, which are related to yield, in addition to lodicule swelling and anther extrusion, which are related to flower opening. These factors may have negative implications for practical wheat breeding. For example, an extremely compact spike combined with a marked increase in spikelet density is undesirable for practical varieties. Regarding resistance to FHB, initial (type I) resistance, which refers specifically to initial infection or invasion (Mesterhazy et al. 1995, 1999), is significantly improved by the cleistogamous (-like) flowering introduced by wheat accession 'U24' as mentioned above (Kubo et al. 2010, 2013). However, segregated genotypes with one or two anthers retained in a floret show higher susceptibility (Kubo et al. 2013). Similarly, other wheat cultivars with partially retained anthers show high susceptibility, whereas cultivars with a high rate of anther extrusion are resistant to the initial infection (Graham and Browne 2009, He et al. 2016 Kubo et al. 2013, Lu et al. 2013). Therefore, 'complete' cleistogamy, as achieved in barley cultivars, is essential for improving initial resistance to FHB in wheat. In this respect, the feasibility of developing complete cleistogamy in wheat is the main challenge, apart from fine-tuning other agronomically important factors.

Fig. III-1 Sequence variation in the miR172 target site in wheat *AP2* homoeologs. Three mutant alleles, *AP2-A1*, *AP2-D1* and *AP2-D2*, identified in EMS-induced mutants of wild-type (WT) 'Kitahonami' have point mutations indicated in red (Chapter II). The predicted amino acid sequences are shown below the corresponding DNA sequences. DDBJ accession numbers: *AP2-A1* (LC772979); *AP2-D1* (LC772981); and *AP2-D2* (LC772982) (Chapter II).

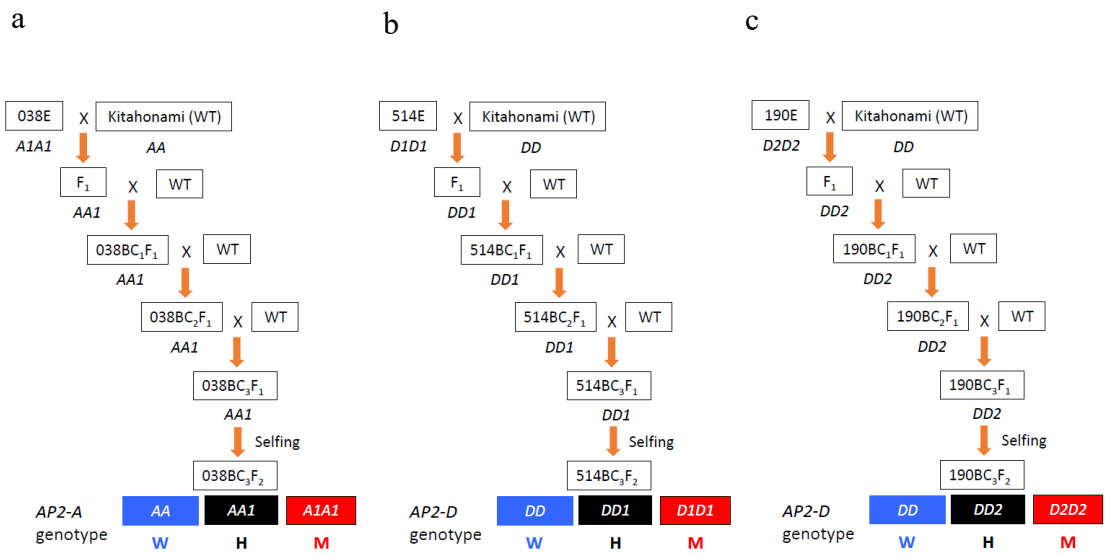

Fig. III-2 Schematic representation of the crosses used to generate NILs carrying three single mutant alleles. $038BC_3F_2$ (**a**), $514BC_3F_2$ (**b**) and $190BC_3F_2$ (**c**) for *AP2-A1*, *AP2-D1* and *AP2-D2* mutant alleles, respectively. Simplified allele symbols are used below the box: *A* and *D* for the wild-type *AP2-A* and *AP2-D* alleles, respectively; *A1*, *D1* and *D2* for the corresponding *AP2* mutant alleles.

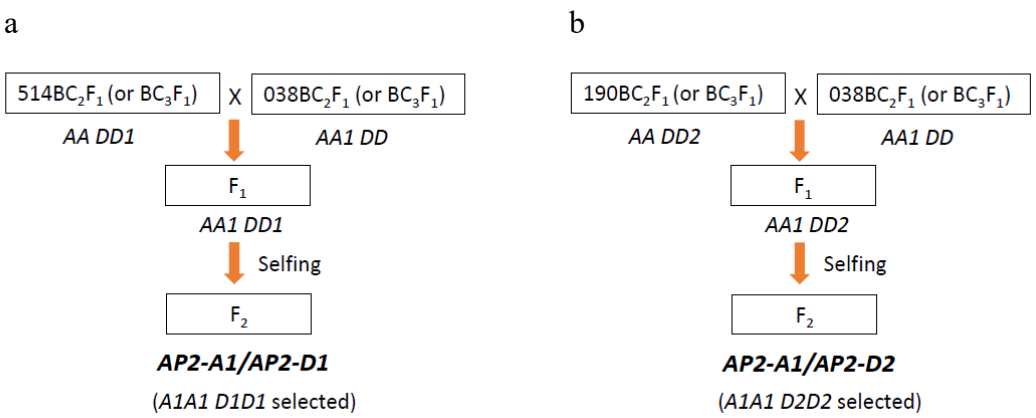

Fig. III-3 Schematic representation of the crosses used to generate double mutants *AP2-A1/AP2-D1* (**a**) and *AP2-A1/AP2-D2* (**b**). See Fig. III-2 for line names and allele abbreviations.

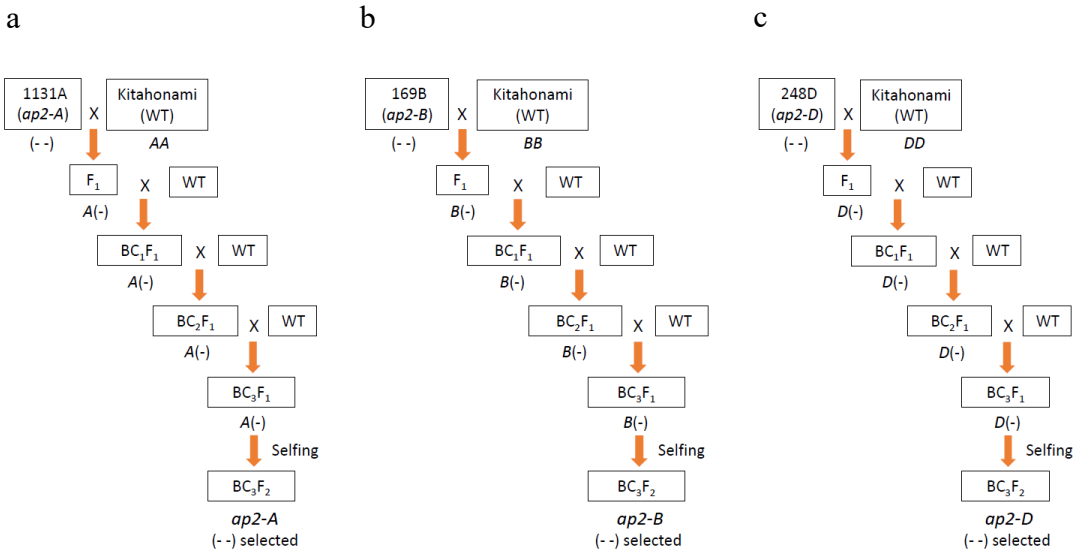

Fig. III-4 Schematic representation of the crosses used to generate NILS carrying three null mutant alleles for *ap2-A* **(a),** *ap2-B* **(b)** and *ap2-D* **(c)**. Simplified allele symbols are used below the box: *A*, *B* and *D* for the wild-type *AP2-A*, *AP2-B* and *AP2-D* alleles, respectively; (-) for each of the corresponding null mutant alleles. *ap2-D*©

Table III-1 Primers and PCR conditions used for genotyping in this study

Table S1 Primers and PCR conditions used for genotyping in this study

Target	Primer	Sequence (5' to 3`)	PCR conditions
AP2-A	F-est1320	TGCACGGCTGGGGCAACGTC	95°C/2 min, (95°C/15 s, 68°C/60 s) × 30 cycles
Deletion	R-HRM A1	CGCGGTGCGCGGTGGTGGAG	
AP2-B	Fw-TaAP2B1	TGCATGGCTGGGGCAACGTC	95°C/2 min, (95°C/15 s, 65°C/60 s) × 30 cycles
Deletion	Rv-TaAP2B1	GACGGATGGTCTCCGGGTAC	
AP2-D	F-est1320	TGCACGGCTGGGGCAACGTC	95°C/2 min, (95°C/15 s, 68°C/60 s) × 30 cycles
Deletion	R-HRM_D2	GCGGTGGAGCTGGTCTTGAT	
AP2-A	A-wt	CGCAGCAGCAGCTGCAGC	95°C/2 min, (95°C/15 s, 68°C/60 s) × 30 cycles
Wild type	R-HRM_A1	CGCGGTGCGCGGTGGTGGAG	
AP2-A1	A-Mut	CGCAGCAGCAGCTGCAGT	95°C/2 min, (95°C/15 s, 66°C/60 s) × 30 cycles
Mutant	R-HRM_A1	CGCGGTGCGCGGTGGTGGAG	
AP2-D	D-wt1	CGCCGCAGCAGCTGCAGC	95°C/2 min, (95°C/15 s, 68°C/60 s) × 27 cycles
Wild type (vs. *D1*)	R-HRM_D2	GCGGTGGAGCTGGTCTTGAT	
AP2-D1	D_mut_T	CGCCGCAGCAGCTGCAGT	95°C/2 min, (95°C/15 s, 68°C/60 s) × 27 cycles
Mutant	R-HRM_D2	GCGGTGGAGCTGGTCTTGAT	
AP2-D	D-wt 2	CCGCCGCAGCAGCTGCAG	95°C/2 min, (95°C/15 s, 68°C/60 s) × 27 cycles
Wild type (vs. *D2*)	R-HRM_D2	GCGGTGGAGCTGGTCTTGAT	
AP2-D2	D_mut2_A	CCGCCGCAGCAGCTGCAA	95°C/2 min, (95°C/15 s, 68°C/60 s) × 27 cycles
Mutant	R-HRM_D2	GCGGTGGAGCTGGTCTTGAT	

* Each 10 μL PCR mixture contains 0.25 U ExTaq DNA polymerase (Takara Bio Inc., Ōtsu, Japan), 1×Ex Taq polymerase buffer, 8% DMSO, 0.3μM of each primer, and template DNA.

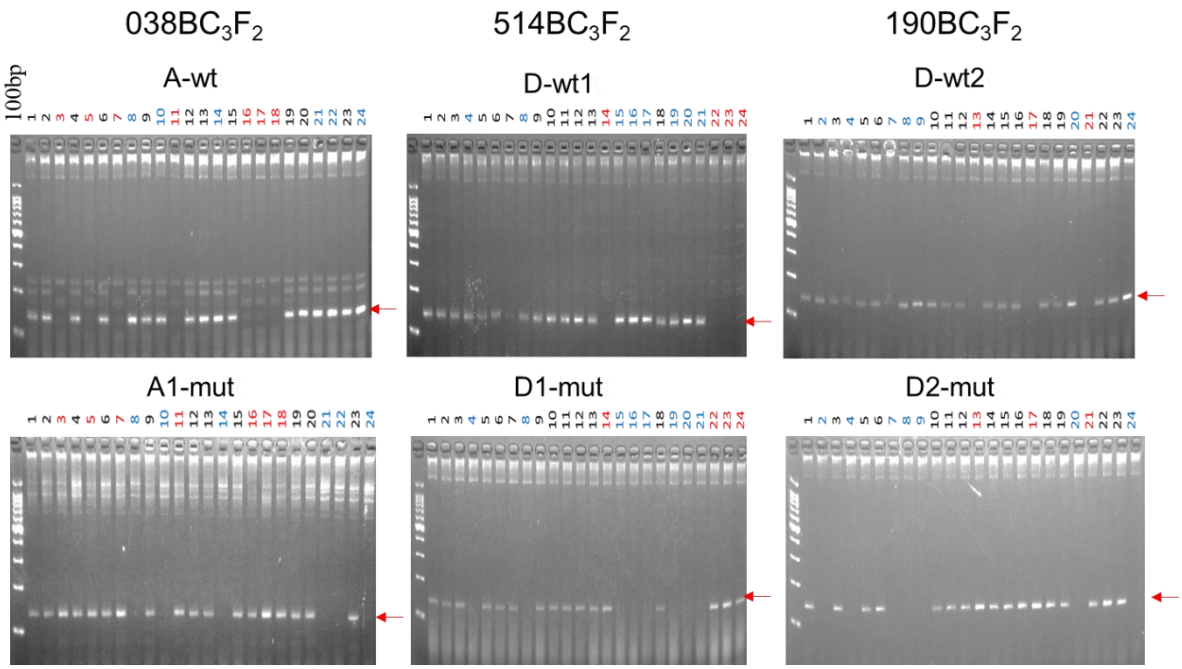

Fig. III-5 Genotyping by allele-specific PCR in three BC_3F_2 NILs. For example, in $038BC_3F_2$, wild-type *AP2-A* and mutant *AP2-A1* alleles were specifically amplified in the A-wt and A1-mut panels, respectively, resulting in the genotyping of individual F_2 plants (no. above the gel) into wild-type homozygotes (blue), heterozygotes (black), and mutant homozygotes (red). Similarly, wild-type *AP2-D* and mutant *AP2-D1* or *AP2-D2* alleles were specifically amplified and genotyped in $514BC_3F_2$ and $190BC_3F_2$. Red arrows indicate the positions of the amplified products.

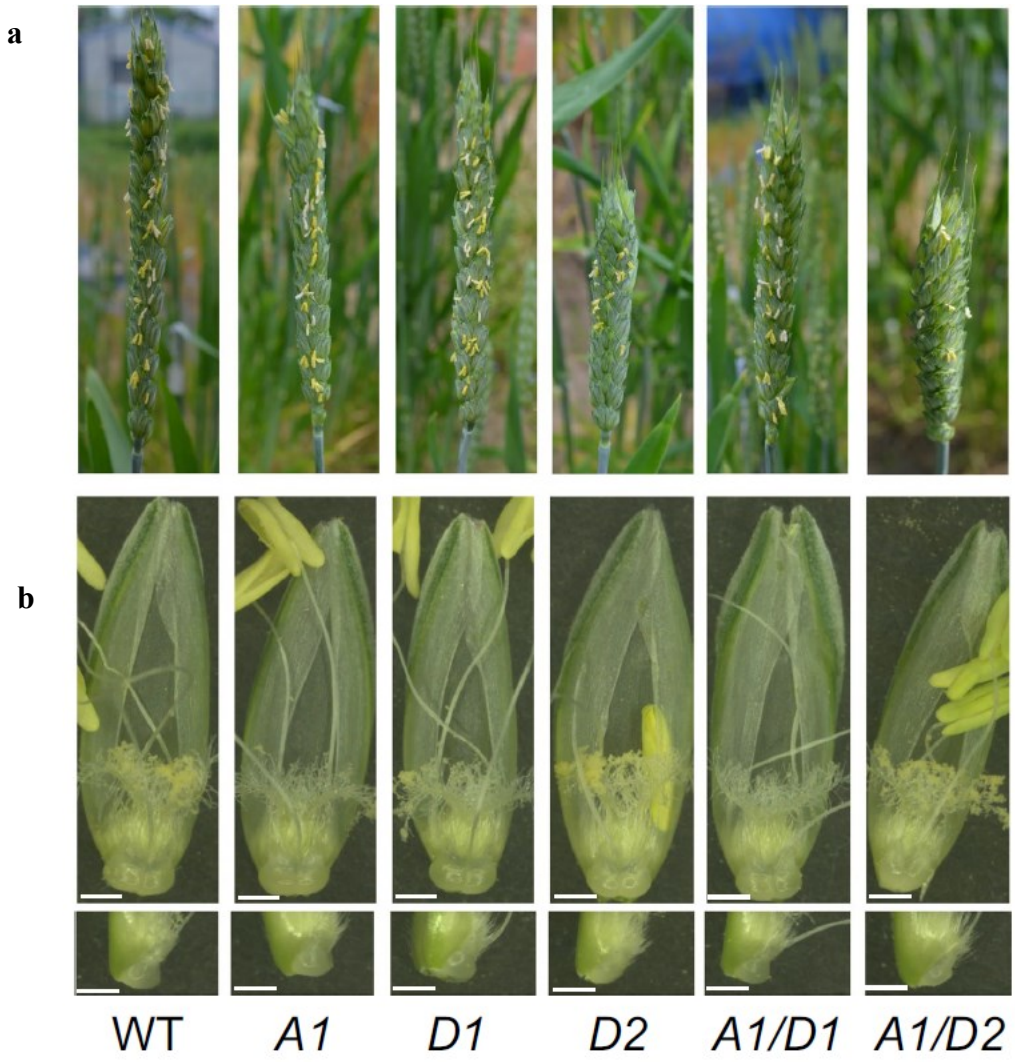

Fig. III-6 Spike and floral organs of wild-type and *AP2* mutants. Spike at anthesis **(a)**, floret at anthesis **(b)** (top panel) and lateral view of the lodicule (bottom panel). Bar, 1 mm. Abbreviations: WT for cv. 'Kitahonami'. *A1*, *D1* and *D2* refer to single mutants *AP2-A1*, *AP2-D1* and *AP2-D2*, respectively, obtained from plants in the BC_3F_2 progeny (Fig. III-2). *A1/D1* and *A1/D2* represent double mutants *AP2-A1*/*AP2-D1* and *AP2-A1*/*AP2-D2*, respectively, obtained from plants in the F_2 progeny of $BC_2F_1 \times BC_2F_1$ (**Fig. III-3**).

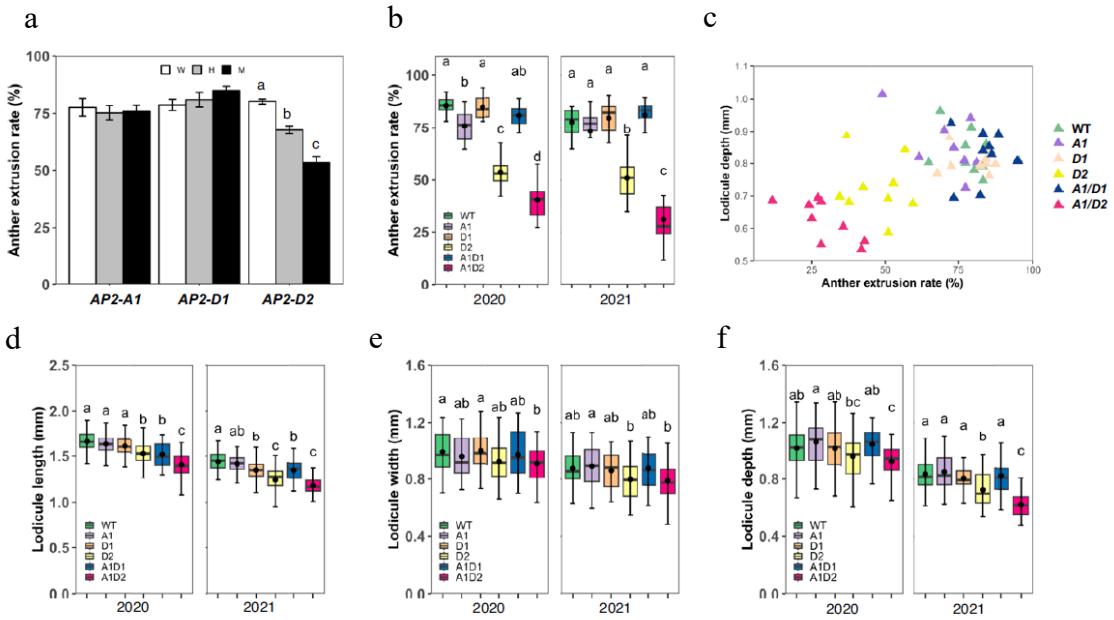

Fig. III-7 Comparison of anther extrusion rate and lodicule size. Comparison of anther extrusion rate among three genotypes (W, H and M) in three NILs of the BC_3F_2 generation segregating for the *AP2-A1*, *AP2-D1* and *AP2-D2* alleles (**a**). Comparison of anther extrusion rate among wild-type and single and double mutants (**b**). Correlation between anther extrusion rate and lodicule depth. Individual plant data from two years (2020–2021) are combined (**c**). Comparison of lodicule size among wild-type, single and double mutants for length (**d**), width (**e**) and depth (**f**). Thick horizontal lines indicate median (50% interquartile range), bullets indicate mean, and whiskers indicate maximum and minimum values excluding outliers. Means with the same letter are not significantly different ($P > 0.05$) according to the Tukey-Kramer HSD test. *Abbreviations*: ***(a)*** W, wild-type *AP2* allele homozygote; H, heterozygote; M, mutant *AP2* allele homozygote; ***(b-f)*** WT for cv. 'Kitahonami'. *A1*, *D1* and *D2* refer to single mutants *AP2-A1*, *AP2-D1* and *AP2-D2*, respectively, taken from plants in the BC_3F_2 (2020) and BC_3F_3 (2021) progeny. *A1/D1* and *A1/D2* represent double mutants *AP2-A1/AP2-D1* and *AP2-A1/AP2-D2*, respectively, taken from plants in the F_2 (2020) and F_3 (2021) progeny of $BC_2F_1 \times BC_2F_1$.

Table III-2 Comparison of spike and floral traits in three NILs of the BC_3F_2 generation segregating for the *AP2-A1*, *AP2-D1* and *AP2-D2* alleles (mean ± S.E)

NIL	Genotype		Anther extrusion	Rachis internode	Seed fertility	Lodicule size					
		n	rate (%)	length (mm)	(%)	*n*	Length (mm)	Width (mm)	Depth (mm)	Relative length	Relative width	Relative depth
038BC_3F_2 *AP2-A1*	W	10	77.6 ± 3.9	4.38 ± 0.01	92.3 ± 1.7	30	1.61 ± 0.02	1.00 ± 0.02	1.01 ± 0.03	0.45 ± 0.01	0.28 ± 0.01	0.28 ± 0.01
	H	10	75.3 ± 3.2	4.28 ± 0.01	90.8 ± 1.6	30	1.57 ± 0.02	0.92 ± 0.02	0.92 ± 0.02	0.44 ± 0.01	0.26 ± 0.01	0.26 ± 0.01
	M	10	76.0 ± 2.7	4.12 ± 0.00	92.9 ± 1.9	60	1.64 ± 0.01	0.96 ± 0.02	1.06 ± 0.02	0.48 ± 0.01	0.28 ± 0.01	0.31 ± 0.00
514BC_3F_2 *AP2-D1*	W	10	78.7 ± 2.5	4.31 ± 0.01	94.8± 1.5	30	1.53 ± 0.02	0.99 ± 0.03	0.99 ± 0.02	0.44 ± 0.01	0.29 ± 0.01	0.29 ± 0.01
	H	10	81.0 ± 3.2	4.12 ± 0.01	97.3 ± 0.9	30	1.58 ± 0.02	0.99 ± 0.03	1.01 ± 0.03	0.43 ± 0.01	0.27 ± 0.01	0.28 ± 0.01
	M	10	85.0 ± 1.8	4.02 ± 0.01	94.4 ± 1.8	60	1.61 ± 0.01	1.00 ± 0.02	1.01 ± 0.02	0.44 ± 0.01	0.27 ± 0.01	0.27 ± 0.01
190BC_3F_2 *AP2-D2*	W	10	80.2 ± 1.1	4.41 ± 0.01	97.9 ± 1.0	30	1.55 ± 0.02	0.95 ± 0.02	1.00 ± 0.02	0.44 ± 0.01	0.27 ± 0.01	0.28 ± 0.01
	H	10	67.7 ± 1.6	3.36 ± 0.01	98.0 ± 0.9	30	1.63 ± 0.02	1.00 ± 0.02	1.09 ± 0.03	0.45 ± 0.01	0.27 ± 0.01	0.30 ± 0.01
	M	10	53.5 ± 2.6	2.76 ± 0.01	94.9 ± 0.8	60	1.54 ± 0.02	0.93 ± 0.02	0.97 ± 0.02	0.41 ± 0.01	0.25 ± 0.00	0.26 ± 0.00

NIL	Genotype		Palea size			Anther size		
		n	Length (mm)	Width (mm)	Length /Width	Length (mm)	Width (mm)	Length /Width
038BC_3F_2 *AP2-A1*	W	15	10.74 ± 0.10	3.61 ± 0.08	3.00 ± 0.07	2.87 ± 0.08	0.83 ± 0.03	3.51 ± 0.11
	H	15	10.91 ± 0.06	3.61 ± 0.08	3.04 ± 0.07	2.71 ± 0.06	0.82 ± 0.02	3.36 ± 0.15
	M	30	10.84 ± 0.09	3.47 ± 0.06	3.15 ± 0.04	2.68 ± 0.05	0.81 ± 0.03	3.46 ± 0.16
514BC_3F_2 *AP2-D1*	W	15	10.63 ± 0.09	3.47 ± 0.07	3.08 ± 0.06	2.92 ± 0.12	0.87 ± 0.04	3.45 ± 0.22
	H	15	10.78 ± 0.08	3.66 ± 0.07	2.96 ± 0.06	3.08 ± 0.08	0.88 ± 0.03	3.53 ± 0.14
	M	30	10.85 ± 0.08	3.73 ± 0.07	2.93 ± 0.05	2.90 ± 0.07	0.93 ± 0.03	3.24 ± 0.14
190BC_3F_2 *AP2-D2*	W	15	10.89 ± 0.04	3.58 ± 0.08	3.07 ± 0.07	2.67 ± 0.09	0.85 ± 0.03	3.15 ± 0.12
	H	15	11.53 ± 0.09	3.65 ± 0.08	3.17 ± 0.06	3.24 ± 0.09	0.86 ± 0.03	3.80 ± 0.11
	M	30	11.38 ± 0.07	3.79 ± 0.07	3.03 ± 0.05	2.95 ± 0.07	0.83 ± 0.03	3.67 ± 0.16

W: wild-type *AP2* allele homozygote, H: heterozygote, M: mutant *AP2* allele homozygote.
n: number of spikes and lodicules used.

Table III-3 Comparison of spike and floral traits between wild-type, single and double *AP2* mutants (mean ± S.E.)

Year	Genotype	*n*	Anther extrusion rate (%)	Rachis internode length (mm)	Rachis length (cm)	No. of Rachis nodes	Seed fertility (%)	*n*	Lodicule size: Length (mm)	Width (mm)	Depth (mm)	Relative length	Relative width	Relative depth
2020	WT	20	85.7 ± 0.9	4.48 ± 0.04	9.32 ± 0.11	20.8 ± 0.3	96.5 ± 0.8	90	1.66 ± 0.01	0.99 ± 0.02	1.02 ± 0.01	0.45 ± 0.01	0.27 ± 0.00	0.28 ± 0.01
	AP2-A1	10	76.0 ± 2.7	4.12 ± 0.04	8.98 ± 0.13	21.8 ± 0.3	92.9 ± 1.9	60	1.64 ± 0.01	0.96 ± 0.02	1.06 ± 0.02	0.48 ± 0.01	0.28 ± 0.00	0.31 ± 0.01
	AP2-D1	10	85.0 ± 1.8	4.02 ± 0.06	8.44 ± 0.15	21.0 ± 0.3	94.4 ± 1.8	60	1.61 ± 0.01	1.00 ± 0.02	1.01 ± 0.02	0.44 ± 0.01	0.27 ± 0.00	0.27 ± 0.01
	AP2-D2	10	53.5 ± 2.6	2.76 ± 0.05	5.96 ± 0.16	21.6 ± 0.3	94.9 ± 0.8	60	1.54 ± 0.02	0.93 ± 0.02	0.97 ± 0.02	0.41 ± 0.01	0.25 ± 0.00	0.26 ± 0.01
	AP2-A1/AP2-D1	12	80.9 ± 1.5	3.88 ± 0.04	8.37 ± 0.16	21.6 ± 0.4	97.6 ± 0.8	30	1.53 ± 0.02	0.98 ± 0.03	1.05 ± 0.02	0.44 ± 0.01	0.28 ± 0.00	0.30 ± 0.01
	AP2-A1/AP2-D2	16	40.3 ± 2.7	2.72 ± 0.04	5.88 ± 0.12	21.6 ± 0.3	94.3 ± 1.1	60	1.42 ± 0.02	0.91 ± 0.02	0.93 ± 0.01	0.38 ± 0.01	0.24 ± 0.00	0.25 ± 0.00
	ANOVA		***	***	***	n.s.	n.s.		***	**	***	***	**	***
2021	WT	21	77.7 ± 1.4	3.95 ± 0.05	8.61 ± 0.13	21.8 ± 0.2	96.3 ± 0.9	36	1.44 ± 0.02	0.87 ± 0.02	0.83 ± 0.02	0.41 ± 0.01	0.25 ± 0.01	0.24 ± 0.01
	AP2-A1	17	73.2 ± 3.0	3.64 ± 0.03	7.76 ± 0.11	21.3 ± 0.8	93.2 ± 2.0	36	1.41 ± 0.02	0.89 ± 0.02	0.85 ± 0.02	0.41 ± 0.01	0.26 ± 0.01	0.25 ± 0.01
	AP2-D1	21	79.7 ± 1.9	3.57 ± 0.04	7.63 ± 0.09	21.4 ± 0.2	95.9 ± 1.2	36	1.35 ± 0.02	0.86 ± 0.02	0.80 ± 0.01	0.40 ± 0.01	0.25 ± 0.01	0.24 ± 0.00
	AP2-D2	20	51.0 ± 2.2	2.42 ± 0.02	5.15 ± 0.07	21.3 ± 0.2	89.8 ± 1.5	36	1.24 ± 0.02	0.80 ± 0.02	0.73 ± 0.02	0.36 ± 0.01	0.23 ± 0.01	0.21 ± 0.01
	AP2-A1/AP2-D1	21	81.1 ± 2.2	3.38 ± 0.04	7.26 ± 0.14	21.4 ± 0.3	89.9 ± 3.0	36	1.35 ± 0.02	0.88 ± 0.02	0.83 ± 0.02	0.39 ± 0.01	0.26 ± 0.01	0.24 ± 0.01
	AP2-A1/AP2-D2	19	31.7 ± 2.5	2.37 ± 0.03	5.03 ± 0.06	21.2 ± 0.2	91.6 ± 1.8	36	1.18 ± 0.02	0.79 ± 0.02	0.62 ± 0.01	0.33 ± 0.01	0.22 ± 0.01	0.17 ± 0.00
	ANOVA		***	***	***	n.s.	n.s.		***	**	***	***	**	***

Year	Genotype	*n*	Palea size: Length (mm)	Width (mm)	Length /Width	Anther size: Length (mm)	Width (mm)	Length /Width
2020	WT	45	10.9 ± 0.04	3.68 ± 0.05	3.00 ± 0.04	2.78 ± 0.09	0.92 ± 0.02	3.10 ± 0.13
	AP2-A1	30	10.8 ± 0.09	3.47 ± 0.06	3.15 ± 0.04	2.68 ± 0.05	0.81 ± 0.03	3.46 ± 0.16
	AP2-D1	30	10.9 ± 0.08	3.73 ± 0.07	2.93 ± 0.05	2.90 ± 0.07	0.93 ± 0.03	3.24 ± 0.14
	AP2-D2	30	11.38 ± 0.07	3.79 ± 0.07	3.03 ± 0.05	2.95 ± 0.07	0.83 ± 0.03	3.67 ± 0.16
	AP2-A1/AP2-D1	15	10.85 ± 0.10	3.53 ± 0.08	3.09 ± 0.05	2.88 ± 0.07	0.88 ± 0.04	3.37 ± 0.20
	AP2-A1/AP2-D2	30	10.94 ± 0.05	3.74 ± 0.05	2.94 ± 0.04	2.78 ± 0.09	0.88 ± 0.02	3.22 ± 0.12
	ANOVA		***	**	*	n.s.	**	**
2021	WT	18	10.67 ± 0.08	3.52 ± 0.10	3.07 ± 0.08	n/a	n/a	n/a
	AP2-A1	18	10.84 ± 0.06	3.46 ± 0.06	3.16 ± 0.06	n/a	n/a	n/a
	AP2-D1	18	10.67 ± 0.06	3.40 ± 0.06	3.16 ± 0.06	n/a	n/a	n/a
	AP2-D2	18	10.65 ± 0.16	3.44 ± 0.08	3.12 ± 0.06	n/a	n/a	n/a
	AP2-A1/AP2-D1	18	10.79 ± 0.04	3.44 ± 0.07	3.16 ± 0.06	n/a	n/a	n/a
	AP2-A1/AP2-D2	18	10.82 ± 0.04	3.57 ± 0.07	3.05 ± 0.06	n/a	n/a	n/a
	ANOVA		***	**	***	n.s.	***	***

*, **, *** and n.s.: significant at 5%, 1%, 0.1% and not significant at 5% levels, respectively.

WT: wild type 'Kitahonami'. *n:* number of spikes, lodicules, paleas and anthers used. n/a: not applicable.

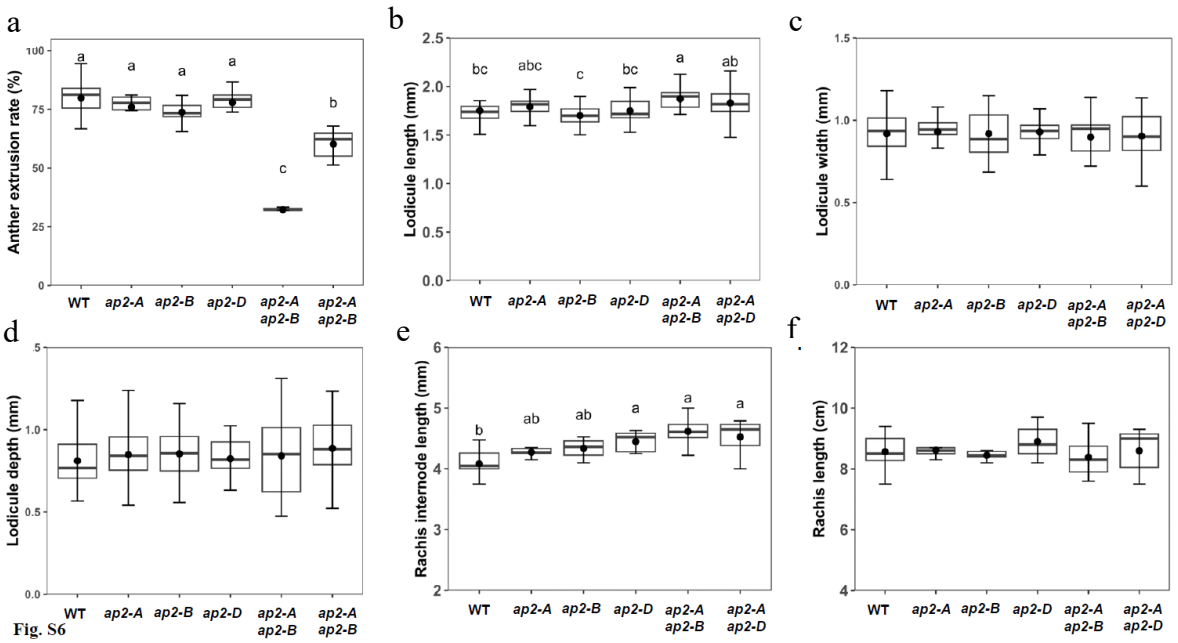

Fig. S6

Fig. III-8 Comparison of the characteristics of wild-type, single and double-null mutants. The anther extrusion rate (**a**), lodicule size for length (**b**), width (**c**), depth (**d**), rachis internode length (**e**), and rachis length (**f**) are shown with data from 2022. *ap2-A*, *ap2-B* and *ap2-D* are null mutants deleted for *AP2-A*, *AP2-B* and *AP2-D* homoeologs, respectively. For abbreviations, see **Fig. III-7** and **Fig. III-4**.

Table III-4 Comparison of spike traits and lodicule size between wild type, single and double null mutants (mean ± S.E)

Genotype		Anther extrusion	Rachis internode	Rachis length	Lodicule size			
	n	rate (%)	length (mm)	(cm)	*n*	Length (mm)	Width (mm)	Depth (mm)
WT	20	79.8 ± 1.6	4.08 ± 0.05	8.57 ± 0.11	24	1.75 ± 0.03	0.92 ± 0.03	0.81 ± 0.03
ap2-A	6	76.0 ± 2.6	4.27 ± 0.03	8.62 ± 0.10	26	1.79 ± 0.02	0.93 ± 0.02	0.85 ± 0.03
ap2-B	6	73.7 ± 2.2	4.34 ± 0.07	8.45 ± 0.06	44	1.70 ± 0.02	0.92 ± 0.02	0.85 ± 0.02
ap2-D	7	77.9 ± 2.5	4.45 ± 0.06	8.90 ± 0.21	28	1.75 ± 0.02	0.93 ± 0.02	0.82 ± 0.02
ap2-A/ap2-B	7	32.3 ± 1.1	4.62 ± 0.09	8.39 ± 0.26	24	1.87 ± 0.03	0.90 ± 0.03	0.84 ± 0.05
ap2-A/ap2-D	7	60.8 ± 2.5	4.52 ± 0.12	8.60 ± 0.29	24	1.83 ± 0.03	0.90 ± 0.03	0.89 ± 0.04
ANOVA		***	***	n.s.		***	n.s.	n.s.

*** and n.s.: significant at 0.1% and not significant at 5% levels, respectively.

WT: wild type 'Kitahonami'. *n:* number of spikes and lodicules used.

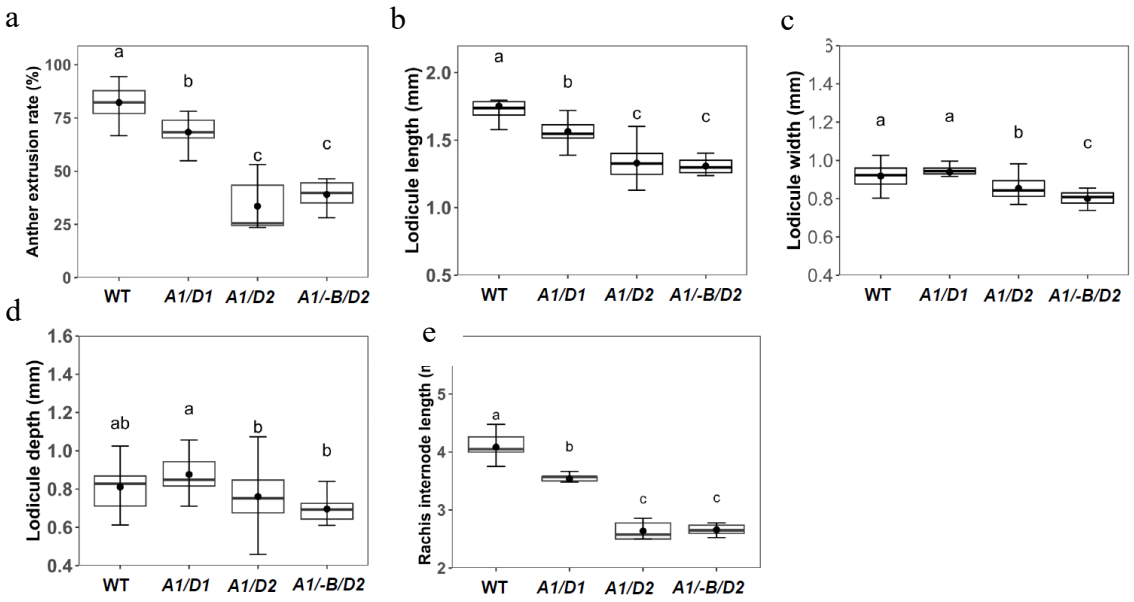

Fig. III-9 Comparison of characteristics between wild-type (WT), *AP2-A1/AP2-D1* (*A1/D1*), and *AP2-A1/AP2-D2* (*A1/D2*) double mutants, and the *AP2-A1/ap2-B/AP2-D2* mutant with the *AP2-B* homoeolog-deleted (*A1/-B/D2*). Anther extrusion rate (**a**), lodicule size for length (**b**), width (**c**), depth (**d**), and rachis internode length (**e**) are shown with data from 2022. For abbreviations, see **Fig. III-7** and **Fig. III-4**.

Table III-5 Anther extrusion rate, rachis internode length and lodicule size in wild-type and three mutant genotypes (mean± S.E)

Genotype		Anther extrusion	Rachis internode	Lodicule size			
					Length	Width	Depth
	n	rate (%)	length (mm)	*n*	(mm)	(mm)	(mm)
WT	20	82.3 ± 1.7	4.08 ± 0.05	12	1.75 ± 0.03	0.92 ± 0.02	0.81 ± 0.03
AP2-A1/AP2-D1	6	68.4 ± 3.4	3.54 ± 0.04	24	1.56 ± 0.02	0.94 ± 0.01	0.88 ± 0.02
AP2-A1/AP2-D2	6	33.5 ± 5.6	2.64 ± 0.07	24	1.33 ± 0.02	0.85 ± 0.01	0.76 ± 0.03
AP2-A1/ap2-B/AP2-D2	7	39.1 ± 2.6	2.66 ± 0.04	12	1.31 ± 0.02	0.80 ± 0.01	0.70 ± 0.02
ANOVA		***	***		***	***	***

***: significant at 0.1%.

WT: wild type 'Kitahonami'. *n:* number of spikes and lodicules used.

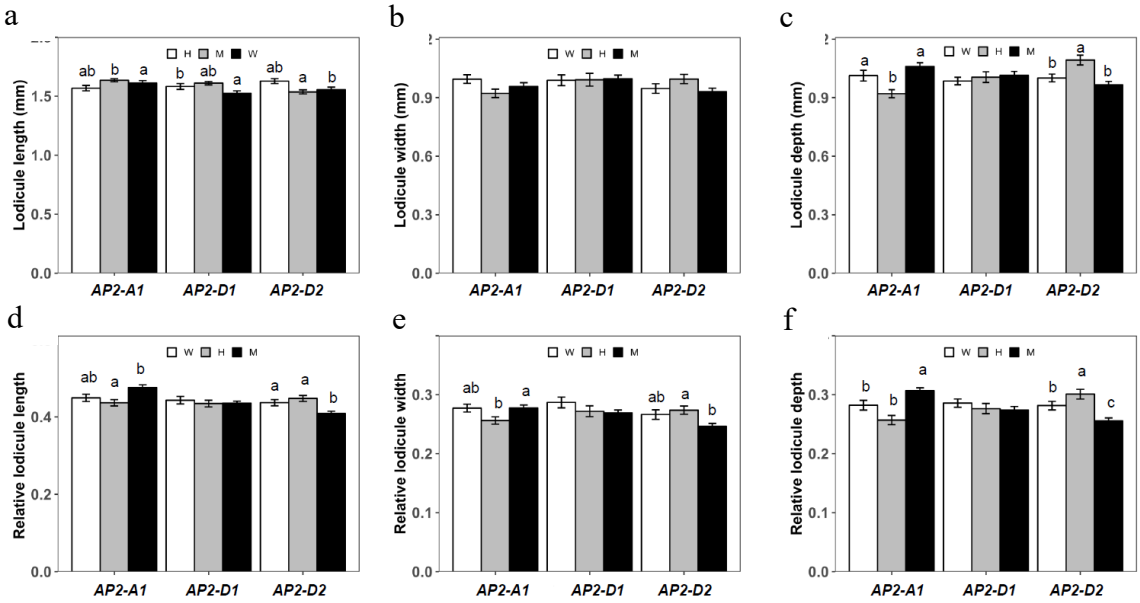

Fig. III-10 The lodicule size in the three NILs of the BC_3F_2 generation segregating for the *AP2-A1*, *AP2-D1* and *AP2-D2* alleles. Lodicule length (**a**), lodicule width (**b**), lodicule depth (**c**), and palea width (**d-f**). Abbreviations: See **Fig. III-7**.

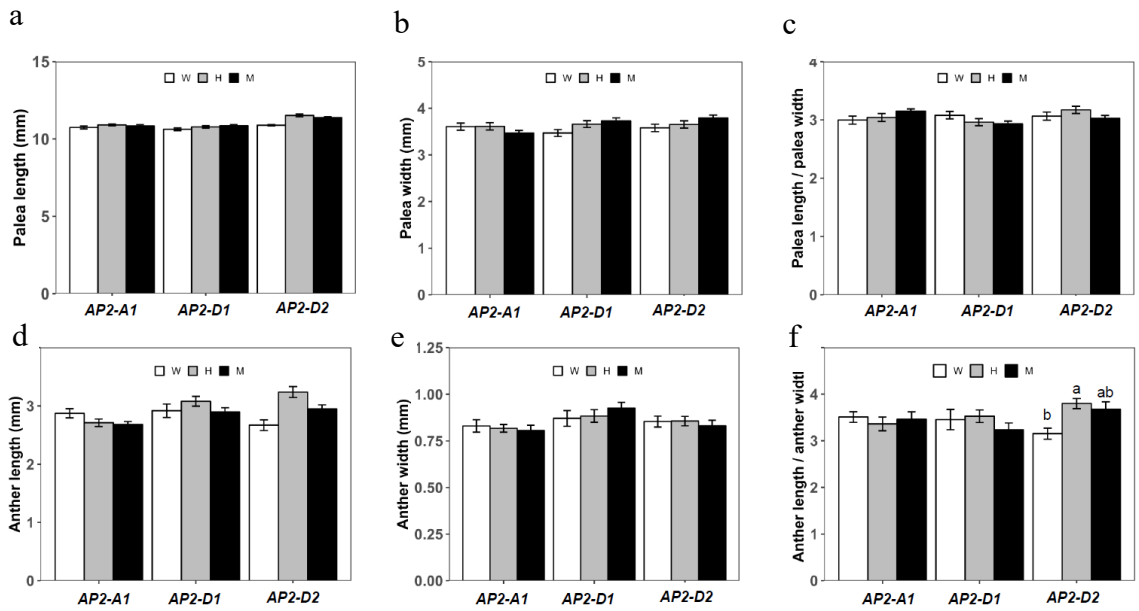

Fig. III-11 Palea and anther sizes in the three NILs of the BC_3F_2 generation segregating for the *AP2-A1*, *AP2-D1* and *AP2-D2* alleles. Palea length (**a**), palea width (**b**), palea length/width (**c**), anther length (**d**), anther width (**e**), and anther length/width (**f**). Abbreviations: See **Fig. III-7**.

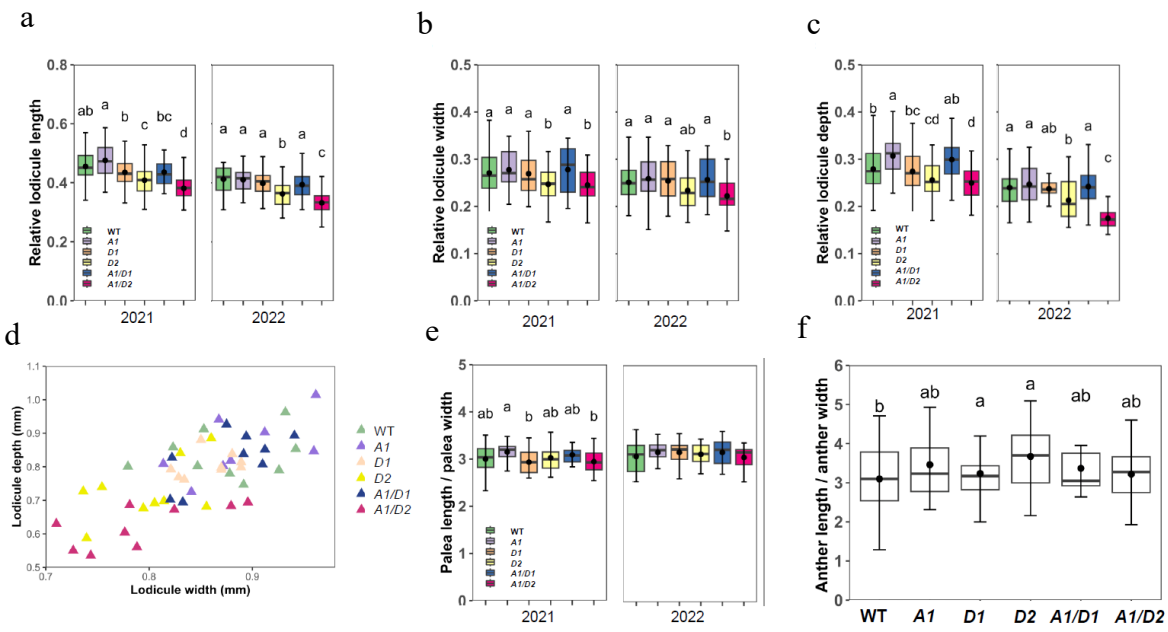

Fig. III-12 Comparison of relative lodicule size and length/width ratio in the palea and anthers between wild type, single, and double mutants. Relative lodicule length (**a**), relative lodicule width (**b**), relative lodicule depth (**c**), and correlations between lodicule width and depth (**d**) are shown. The length/width ratios are shown for the palea (**d**) and anthers (**f**). Abbreviations: See **Fig. III-7**.

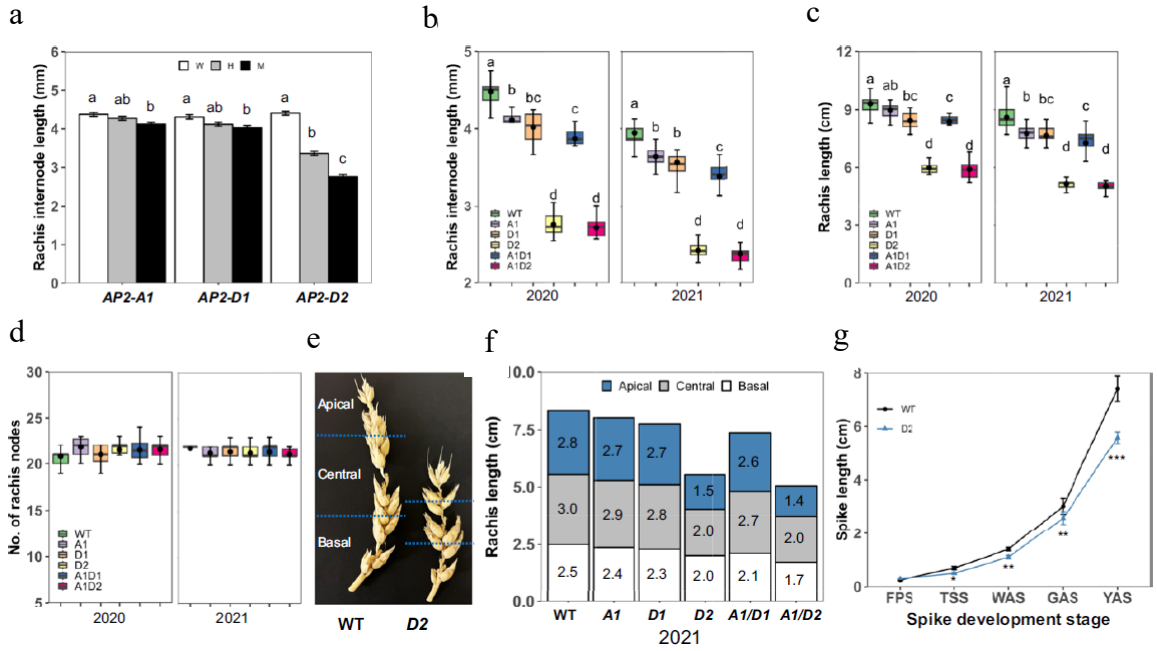

Fig. III-13 Comparison of spike rachis characteristics. Comparison of rachis internode length among three genotypes (W, H and M) in three NILs of the BC_3F_2 generation segregating for the *AP2-A1*, *AP2-D1* and *AP2-D2* alleles (**a**). Comparison of rachis internode length (**b**), rachis length (**c**) and number of rachis nodes (**d**) among wild-type, single and double mutants. Thick horizontal lines indicate median (50% interquartile range), bullets indicate mean, and whiskers indicate maximum and minimum values excluding outliers. Means with the same letter are not significantly different ($P > 0.05$) according to the Tukey-Kramer HSD test. Mature spike showing the basal, central and apical positions on a spike **(e)**. Rachis length in three different positions (basal, central and apical) on a spike **(f)**. Spike length during spike development **(g)**. FPS, floret primordium stage; TSS, terminal spikelet stage; WAS, white anther stage; GAS, green anther stage; YAS, yellow anther stage. *, ** and *** indicate significant differences at 5%, 1% and 0.1% level by t-test. *Abbreviations*: ***(a)*** W, wild-type *AP2* allele homozygote; H, heterozygote; M, mutant *AP2* allele homozygote ; ***(b-g)*** WT for cv. 'Kitahonami'. *A1*, *D1* and *D2* refer to single mutants *AP2-A1*, *AP2-D1* and *AP2-D2*, respectively, taken from plants in the progeny of BC_3F_2 (2020), BC_3F_3 (2021). *A1/D1* and *A1/D2* represent double mutants *AP2-A1*/*AP2-D1* and *AP2-A1*/*AP2-D2*, respectively, taken from plants in the F_2 (2020) and F_3 (2021) progeny of $BC_2F_1 \times BC_2F_1$.

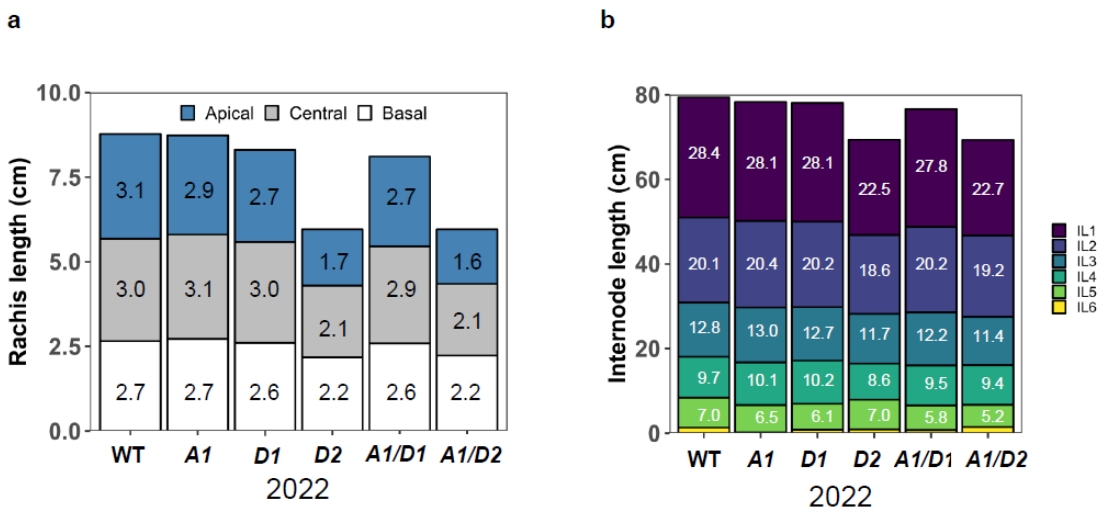

Fig. III-14 Positional variation in rachis and culm lengths. Rachis lengths at three positions (apical, central and basal) on the spike (**a**) and culm internode length (IL1-6) (**b**) are shown with data from 2022. For abbreviations, see **Fig. III-13** and **Fig. III-15**.

Table III-6 Comparison of rachis length at three positions on the spike (mean± S.E)

Year	Genotype	*n*	Rachis length (cm)	Rachis length at different positions		
				Apical (cm)	Central (cm)	Basal (cm)
2021	WT	15	$8.33^{a} \pm 0.22$	$2.80^{a} \pm 0.06$	$3.04^{a} \pm 0.07$	$2.49^{a} \pm 0.03$
	AP2-A1	15	$8.07^{a} \pm 0.16$	$2.73^{ab} \pm 0.05$	$2.92^{ab} \pm 0.05$	$2.36^{ab} \pm 0.03$
	AP2-D1	15	$7.77^{ab} \pm 0.27$	$2.67^{ab} \pm 0.03$	$2.80^{b} \pm 0.06$	$2.29^{bc} \pm 0.04$
	AP2-D2	14	$5.53^{c} \pm 0.15$	$1.49^{c} \pm 0.03$	$2.04^{c} \pm 0.04$	$2.00^{d} \pm 0.04$
	AP2-A1/AP2-D1	13	$7.13^{b} \pm 0.18$	$2.55^{b} \pm 0.04$	$2.71^{b} \pm 0.04$	$2.11^{cd} \pm 0.07$
	AP2-A1/AP2-D2	11	$5.41^{c} \pm 0.10$	$1.37^{c} \pm 0.06$	$1.97^{c} \pm 0.06$	$1.72^{e} \pm 0.06$
2022	WT	15	$8.53^{a} \pm 0.12$	$3.09^{a} \pm 0.08$	$3.03^{a} \pm 0.11$	$2.65^{a} \pm 0.04$
	AP2-A1	15	$8.30^{a} \pm 0.15$	$2.93^{ab} \pm 0.07$	$3.08^{a} \pm 0.04$	$2.72^{a} \pm 0.06$
	AP2-D1	15	$7.63^{b} \pm 0.12$	$2.72^{bc} \pm 0.04$	$2.99^{a} \pm 0.05$	$2.60^{a} \pm 0.06$
	AP2-D2	15	$5.40^{c} \pm 0.13$	$1.67^{d} \pm 0.04$	$2.12^{b} \pm 0.05$	$2.17^{b} \pm 0.05$
	AP2-A1/AP2-D1	15	$7.57^{b} \pm 0.15$	$2.65^{c} \pm 0.05$	$2.87^{a} \pm 0.04$	$2.59^{a} \pm 0.04$
	AP2-A1/AP2-D2	15	$5.53^{c} \pm 0.13$	$1.61^{d} \pm 0.04$	$2.12^{b} \pm 0.03$	$2.23^{b} \pm 0.03$

Means with the same letter are not significantly different ($P > 0.05$) according to the Tukey-Kramer HSD test.

WT: wild type 'Kitahonami'. *n:* number of culms used.

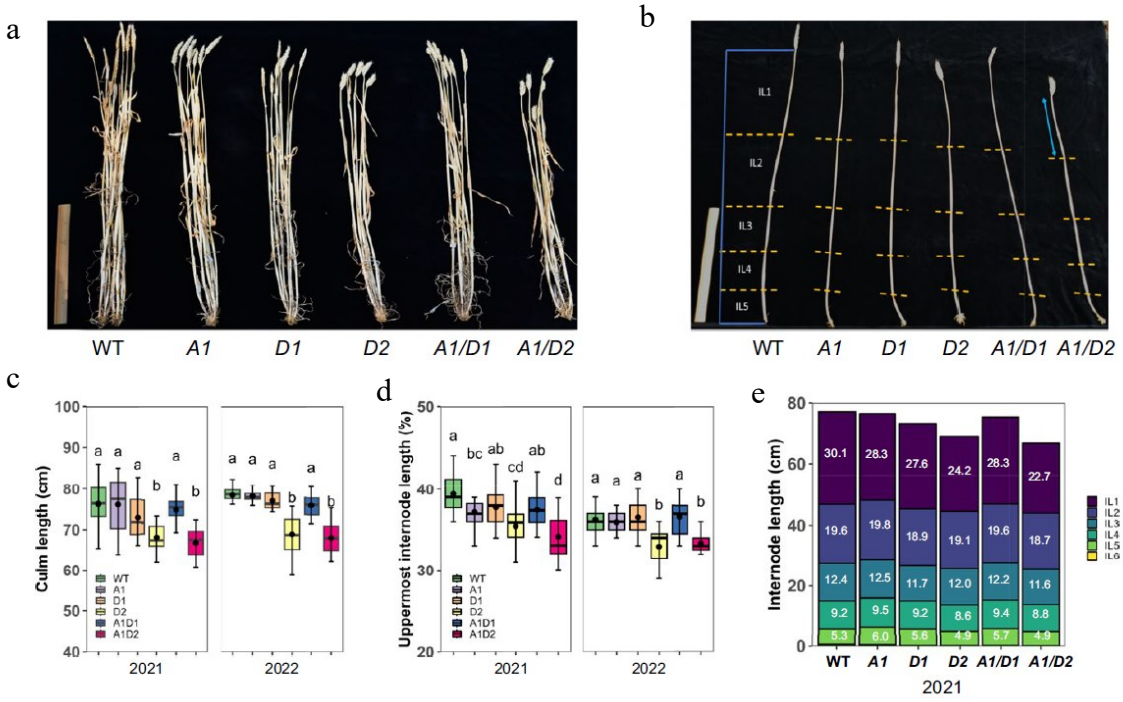

Fig. III-15 Comparison of the culm and its internode length. Appearance of individual plants after harvest **(a)**. Bar, 30 cm. Individual culms with position of each node and internode length (IL) **(b)**. Bar, 30 cm. Culm length **(c)**. Percentage ratio of the length of the uppermost internode (IL1) to culm length (d). Culm length divided by each internode length (IL) (e). In (**c**) and (**d**), thick horizontal lines indicate median (50% interquartile range), bullets indicate mean, and whiskers indicate maximum and minimum values excluding outliers. Means with the same letter are not significantly different ($P > 0.05$) according to the Tukey-Kramer HSD test. *Abbreviations*: WT for cv. 'Kitahonami'. *A1*, *D1* and *D2* refer to single mutants *AP2-A1*, *AP2-D1* and *AP2-D2*, respectively, taken from plants in the BC_3F_3 (2021) and BC_3F_4 (2022) progeny. *A1/D1* and *A1/D2* represent double mutants *AP2-A1*/*AP2-D1* and *AP2-A1*/*AP2-D2*, respectively, taken from plants in the F_3 progeny of $BC_2F_1 \times BC_2F_1$ (2021) and the F_3 progeny of $BC_3F_1 \times BC_3F_1$ (2022).

Table III-7 Comparison of the culm and it's internode length (mean ± S.E)

Year	Genotype		Culm length	Culm internode length						
					IL1	IL2	IL3	IL4	IL5	IL6
		n	(cm)	*n*	(cm)	(cm)	(cm)	(cm)	(cm)	(cm)
2021	WT	24	$78.4^{a} \pm 0.6$	15	$30.1^{a} \pm 0.5$	$19.6^{ab} \pm 0.3$	$12.4^{a} \pm 0.3$	$9.2^{abc} \pm 0.2$	$5.3^{a} \pm 0.4$	$0.5^{a} \pm 0.2$
	AP2-A1	24	$78.2^{a} \pm 0.5$	15	$28.3^{b} \pm 0.5$	$19.8^{a} \pm 0.3$	$12.5^{a} \pm 0.3$	$9.5^{a} \pm 0.2$	$6.0^{a} \pm 0.4$	$0.4^{a} \pm 0.2$
	AP2-D1	24	$77.1^{a} \pm 0.5$	15	$27.6^{b} \pm 0.5$	$18.9^{ab} \pm 0.3$	$11.7^{a} \pm 0.2$	$9.2^{abc} \pm 0.1$	$5.6^{a} \pm 0.3$	$0.2^{a} \pm 0.1$
	AP2-D2	24	$68.9^{b} \pm 1.7$	15	$24.2^{c} \pm 0.3$	$19.1^{ab} \pm 0.2$	$12.0^{a} \pm 0.2$	$8.6^{c} \pm 0.2$	$4.9^{a} \pm 0.3$	$0.2^{a} \pm 0.1$
	AP2-A1/AP2-D1	24	$76.0^{a} \pm 0.8$	15	$28.3^{b} \pm 0.4$	$19.6^{ab} \pm 0.2$	$12.2^{a} \pm 0.1$	$9.4^{ab} \pm 0.1$	$5.7^{a} \pm 0.2$	$0.2^{a} \pm 0.1$
	AP2-A1/AP2-D2	24	$68.0^{b} \pm 1.0$	15	$22.7^{c} \pm 0.3$	$18.7^{b} \pm 0.2$	$11.6^{a} \pm 0.2$	$8.8^{bc} \pm 0.2$	$4.9^{a} \pm 0.3$	$0.1^{a} \pm 0.1$
2022	WT	24	$76.3^{a} \pm 1.1$	15	$28.4^{a} \pm 0.4$	$20.1^{ab} \pm 0.2$	$12.8^{a} \pm 0.2$	$9.7^{ab} \pm 0.2$	$7.0^{a} \pm 0.4$	$1.3^{a} \pm 0.5$
	AP2-A1	24	$76.2^{a} \pm 1.3$	15	$28.1^{a} \pm 0.2$	$20.4^{a} \pm 0.2$	$13.0^{a} \pm 0.2$	$10.1^{a} \pm 0.2$	$6.5^{a} \pm 0.3$	$0.2^{a} \pm 0.1$
	AP2-D1	24	$73.0^{a} \pm 1.1$	15	$28.1^{a} \pm 0.3$	$20.2^{a} \pm 0.2$	$12.7^{ab} \pm 0.1$	$10.2^{ab} \pm 0.3$	$6.1^{a} \pm 0.3$	$0.8^{a} \pm 0.4$
	AP2-D2	24	$68.0^{b} \pm 0.7$	15	$22.5^{b} \pm 0.5$	$18.6^{c} \pm 0.2$	$11.7^{ab} \pm 0.2$	$8.6^{b} \pm 0.2$	$7.0^{a} \pm 1.3$	$0.9^{a} \pm 0.4$
	AP2-A1/AP2-D1	24	$75.1^{a} \pm 0.7$	15	$27.8^{a} \pm 0.4$	$20.2^{a} \pm 0.2$	$12.5^{ab} \pm 0.2$	$9.5^{ab} \pm 0.2$	$5.8^{a} \pm 0.5$	$0.7^{a} \pm 0.4$
	AP2-A1/AP2-D2	24	$66.6^{b} \pm 0.9$	15	$22.7^{b} \pm 0.3$	$19.2^{bc} \pm 0.3$	$11.4^{b} \pm 0.7$	$9.4^{ab} \pm 0.7$	$5.2^{a} \pm 0.3$	$1.5^{a} \pm 0.7$

Means with the same letter are not significantly different ($P > 0.05$) according to the Tukey-Kramer HSD test.

WT: wild type 'Kitahonami'. *n:* number of culms used.

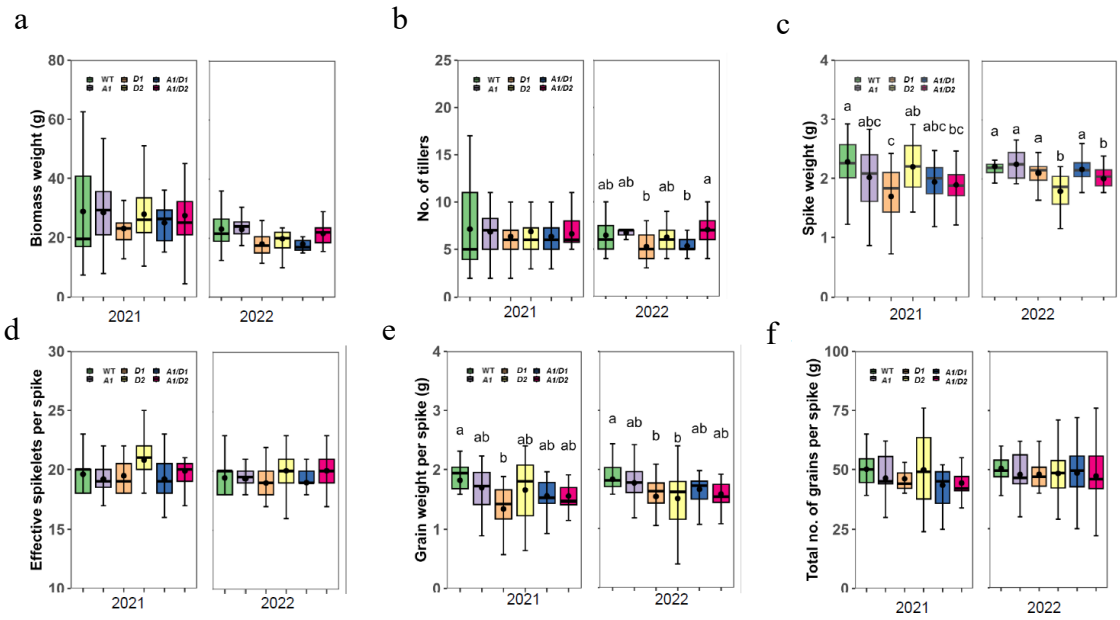

Fig. III-16 Comparison of yield-related traits between wild-type and single and double mutants. Biomass weight (**a**), number of tillers (**b**), spike weight (**c**), effective number of spikelets per spike (**d**), grain weight per spike (**e**), and total number of grains per spike (**f**) are shown along with the data for 2021 and 2022. Abbreviations: See **Fig. III-15**.

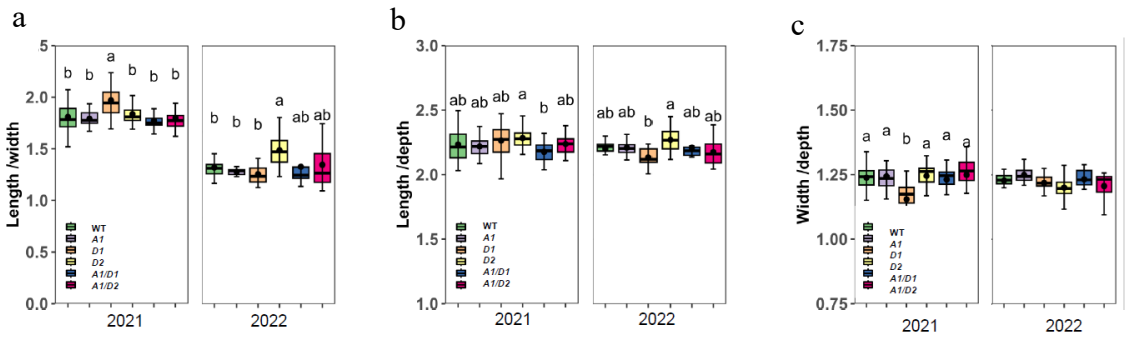

Fig. III-17 Comparison of grain ratios between wild-type, single, and double mutants. The length/width (**a**), length/depth (**b**), and width/depth (**c**) ratios of single grains are shown with data from 2021 and 2022. Abbreviations: See **Fig. III-15**.

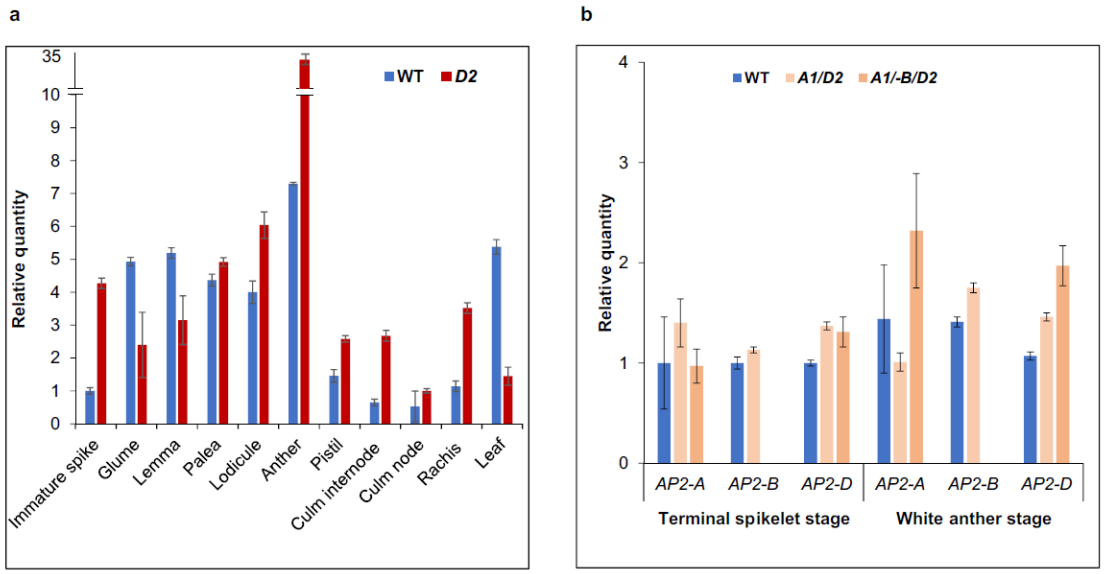

Fig. III-18 Expression analysis of *AP2* homoeologs. Comparison of the transcript abundance of the *AP2-D* homoeolog between different floral organs and plant tissues in the wild type (WT) and the single mutant *AP2-D2* (*D2*). Transcript abundances were normalized to that of *actin* and the immature WT spike (terminal spikelet stage) **(a)**. Transcript abundance of three *AP2* homoeologs (*AP2-A*, *AP2-B* and *AP2-D*) in immature spikes at the terminal spikelet stage (left) and the white anther stage (right). qPCR was performed for each *AP2* homoeolog in the wild type (WT), the *AP2-A1/AP2-D2* (*A1/D2*) double mutant and the *AP2-A1/ap2-B/AP2-D2* mutant with the *AP2-B* homoeolog deleted (*A1/-B/D2*). Transcript abundances were normalized to that of *actin* and WT at the terminal spikelet stage **(b)**.

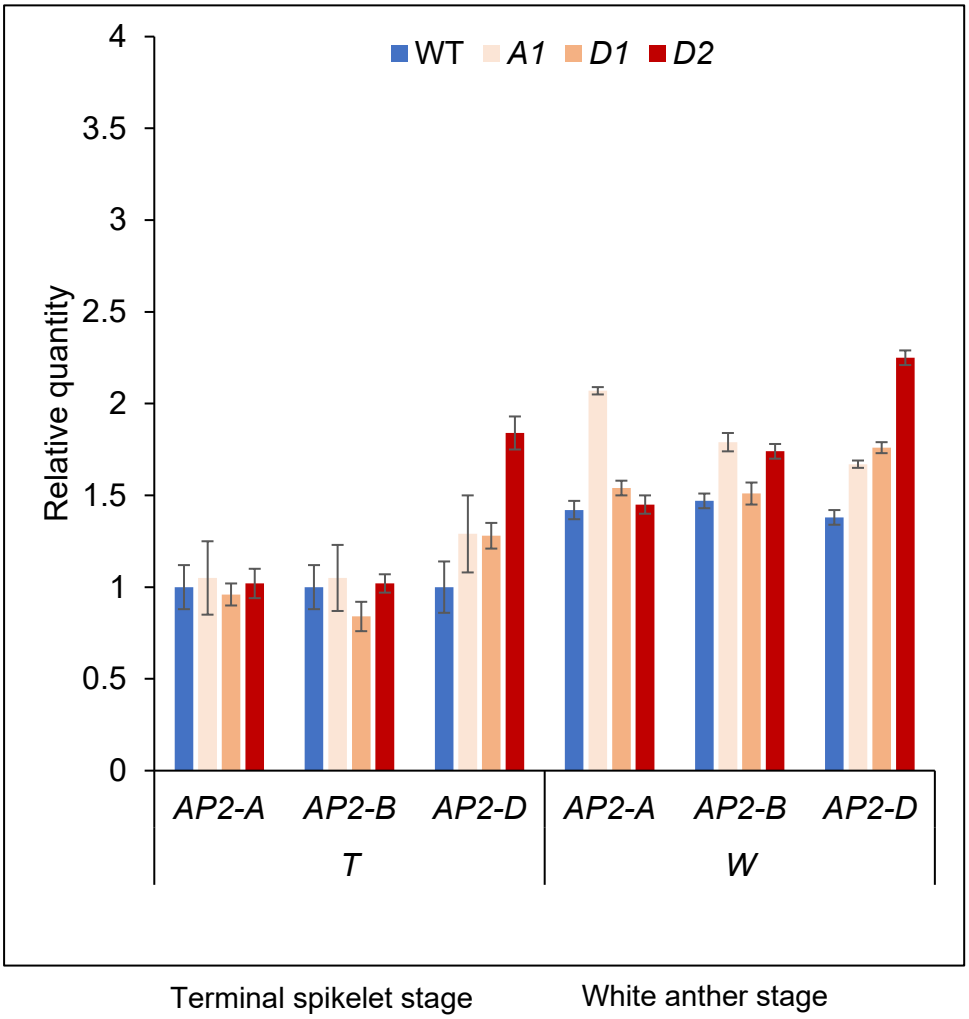

Fig. III-19 Transcript abundance of three *AP2* homoeologs (*AP2-A*, *AP-B* and *AP2-D*) in immature spikes at the terminal spikelet (left) and white anther (right) stages. qPCR was performed for each *AP2* homoeolog in the wild type (WT) and three single mutants (*AP2-A1*, *AP2-D1* and *AP2-D2*). Transcript abundance was normalized to *actin* and WT at the terminal spikelet stage.

a

AP2L5

```
                    5′                          3′
AP2L5(Aq,B,D)       CTGCAGCATCATCAGGATTCT
                    A  A  A  S  S  G  F

AP2L-A5(Q)          CTGCAGCATCATCAGGATTTT
                    A  A  A  S  S  G  F
AP2L-A5(Q′)         CTGCAGCATCATCAGAATTTT
                    A  A  A  S  S  E  F
AP2L-A5(QC1)        CTGCAGCATTATCAGGATTTT
                    A  A  A  L  S  G  F
```

AP2L-B2 (*AP2-B*)

b

```
                    5′                          3′
Ap2l-B2 wt          CCGCAGCATCATCACGATTCC
                    A  A  A  S  S  R  F

rAp2l-B2            CCGCAGCATCATCACAATTCC
                    A  A  A  S  S  Q  F
```

Fig. III-20 Sequence variations in the miR172 target site of wheat *AP2-like* (*AP2L*) genes. *AP2L5* (*Aq*, *B*, *D*) for the wild-type allele with three *AP2L-A5* alleles **(a)**: *Q* (Simons et al. 2006), *Q'* (Greenwood et al. 2017) and Q^{C1} (Xu et al. 2018). Gene symbols followed those described by Debernardi et al. (2020). *AP2L-B2*, referred to as the *AP2L2* gene on chromosome 2B, corresponds to the *AP2-B* homoeolog **(b)**. An induced mutant allele (*rAP2l-B2*) recently identified by Debernardi et al. (2020) is shown with the wild-type allele (*Ap2l-B2* wt). The predicted amino acid sequences are shown below the corresponding DNA sequences.

Chapter IV

General discussion

Mutations in the miR172 target site of wheat AP2 homoeologs inhibit lodicule development and reduces anther extrusion

Lodicules are an important morphological feature in the grass family (*Poaceae*), which includes major cereal crops like wheat, rice, and maize. They are a key part of the reproductive system in Triticeae crops and play a major role in the opening of the grass flower during anthesis (Kosina 2010, Saunders 2024). Lodicules are small, translucent structures at the base of the ovary in grass flowers. They are believed to be a rudimentary periant, or remnants of the sepals in the flower and function by swelling rapidly when the flower is mature (Kosina 2010). Lodicule swelling is the main factor that opens flowers at anthesis in wheat and other cereals by pushing apart the lemma and palea and have been subjects of several studies (Yoshida et al. 2007, Nair et al. 2010, Ning et al. 2013a, Ohmori et al. 2018). Yin (2002) and Kosina (2010) both explored the morphological and developmental aspects of lodicules in wheat, noting the leafy nature of these organs and describing their structure and changes during flowering.

The miR172 target site is a crucial element in the regulation of various physiological and developmental processes in Triticeae crops. The miR172-*APETALA2* (*AP2*) pathway plays a crucial role in the regulation of flowering time and floral organ development in barley and wheat (Jung et al. 2014, Zhao et al. 2015, Patil et al. 2019, Debernardi et al. 2020, 2022, Shoesmith et al. 2021). Debernaridi et al (2020) showed that in wheat, mutations in the miR172 target site of *AP2L* and *Q* genes can alter floret development. The balance in the expression of miR172 and *AP2*-like genes is crucial for the correct development of spikelets and floret, hence, *AP2L5* and *AP2L2* are critical for

axillary floral meristems and lemma identity and mutations in *AP2L2* miR172 target site led to smaller lodicules. Elevated accumulation of miRNA172 leads to floral organ identity defects, similar to those observed in apetala2 loss-of-function mutants. The regulation of *APETALA2* by miRNA172 is specific to its interaction with the mRNA, as evidenced by the effects of mutant *APETALA2* RNA with disrupted miRNA172 base pairing (Chen et al. 2004). *HvAPETALA2* (*HvAP2*) controls floret organ identity, floret boundaries, and maternal tissue differentiation during grain development in barley. A gain-of-function *HvAP2* allele can mask changes in floret organ identity caused by the loss of HvBOP2 gene function. (Shoesmith et al. 2021). A sequence polymorphism at the miR172 target site within *cly1* reduced the abundance of the CLY1 protein, enabling open flowering in barley. A mutant lacking mature miR172a has very small lodicules, resulting in cleistogamous flowering (Anwar et al. 2018). These findings highlight the significance of the miR172-AP2 pathway in the control of flowering and floral development in barley and wheat.

Differences in miR172-guided cleavage of *Cly1* transcripts alter lodicule development and the consequent occurrence of cleistogamy (Nair *et al.* 2010). Importantly, similar mutations replace a strong G:C pair in the WT with a G:U wobble pair in *AP2-A1* and *AP2-D1* and an A:C mismatch in *AP2-D2* (Varani and McClain 2000, Rehmsmeier et al. 2004) in the miR172 interactions, which could maintain weak interactions. The interaction in miR172 is much more reduced in *AP2-D2* than in *AP2-A1* and *AP2-D1* (Chapter II. The differences in interactions with miR172 could also affect the amount of AP2 protein translated, which is necessary for suppressing the development of lodicules (Chapter III).

Lodicule size, particularly depth, was significantly reduced in all three mutants carrying a point mutation of wheat *AP2* homoeologs. The greatest reduction in lodicule

depth was seen in the *AP2-D2* mutant, indicating that this mutation had larger functional effects than the other two mutations (Chapter II). A more effective evaluation using near isogenic lines (NILs) showed that *AP2-D2* allele had the most significant impact on lodicule depth only, among the three single mutant alleles. However, *AP2-A1/AP2-D2* exhibited stronger effect in reducing lodicule size than *AP2-D2* (Chapter III*)*. This demonstrated that a weak *AP2-A1* allele, combined with an effective *AP2-D2* allele, can have a stronger effect on lodicule size reduction than a single *AP2-D2* mutant. However, the accumulation of two weaker alleles (*AP2-A1* and *AP2-D1*) was found to be inadequate in significantly reducing lodicule size (Chapter III). Moreover, none of the mutants, including the double mutants flowered closed. Cleistogamous barley cultivars carrying a natural variant allele, *cly1.b* or *cly1.c*, are characterized by failure of lodicule development and virtually no loss of swelling (Honda et al. 2005, Nair et al. 2010, Wang et al. 2013, 2021). In marked contrast, the double mutant *AP2-A1/AP2-D2* had swollen, although not complete, lodicules with apparent vascular tissue. Thus, the accumulation effect of the two *AP2* homoeologs was insufficient to achieve wheat cleistogamy. This result implies a universal mechanical function of lodicule depth subject to point mutations in the miR172-targeting site in barley and wheat. The pronounced effect of the *AP2-D2* allele on lodicule size can be attributed to its significantly lower interaction with miR172 at the target site (Chapter II). This reduces the likelihood of miR172-mediated mRNA cleavage, resulting in higher transcript levels than from the *AP2-A1*, *AP2-D1*, and WT alleles. The results of qPCR analysis support this, showing high *AP2-D2* transcript levels at both spike development stages (Chapter III).

By Sequencing of *AP2L2* homoeologs Debernardi et al (2019) revealed a single nucleotide polymorphism (SNP) inside the miR172 target region of the *Ap2L-B2* gene, (hencefort *rAp2l-B2*). This mutation exerts a more pronounced impact on miR172

activity due to its elevated free energy of interaction (29.7 kcal/mol) and results in a 30% reduction in lodicule size. This is similar to *AP2-D2* allele effect on lodicule size reduction and reduced minimum free energy interaction within the miR172 target site (Chapter II). The expression analysis reveals that *AP2-D2* exhibits higher transcription levels in the lodicule compared to other floral organs (Chapter III). This finding suggests a correlation between reduced minimum free energy, transcript levels and the reduction in lodicule size. Lower minimum free energy results in higher transcript levels of *AP2-D2* in the lodicule are associated with a greater reduction in lodicule size. Therefore, it can be inferred that the reduced activity *of AP2-D2* allele and the transcriptional activity of *AP2-D2* plays a role in regulating lodicule size during floral development.

An intriguing induced cleistogamous wheat mutant has been reported. The lodicules of the cleistogamous mutant (*ZK001*) did not absorb water, resulting in smaller lodicules, whereas the lodicules of the non-cleistogamous parent cultivar (YM18) expanded normally. Lower calcium and potassium contents were found in the lodicules of *ZK001* than in YM18, which are presumed to be responsible for osmotic adjustments and signal transduction related to water absorption and lodicule expansion. In addition, *ZK001* had a low GA content and a high JA content in the lodicules, leading to reduced size (Tang et al. 2020). There was no information reported on sequence polymorphisms in the *AP2* homoeologs of *ZK001*, but it can be speculated that the mutation(s) induced in *ZK001* is not likely to be associated with *AP2* homoeologs. Rather, it is assumed that mutations induced in *ZK001* occurred in a distinct gene and not likely to be associated with *AP2* homoeologs. Because *ZK001* was obtained from a single mutagenesis event (via static magnetic field), the point mutations within the miR172 targeting site would not be expected to occur simultaneously in all three *AP2* homoeologs. It is also unexpected that deleterious (or

unfunctional) mutations in any of the *AP2* homoeologs would confer cleistogamy as predicted from the present investigation of deletion mutants. Rather, it is assumed that mutations occurred in a distinct gene that encodes an essential regulatory factor specifically involved in the pathway for lodicule development or expansion.

The wheat cultivar 'U24' was once considered cleistogamous wheat (Ueno and Itoh 1997, Kubo et al. 2010), but has been re-evaluated and found to have fully swollen lodicules at anthesis. Although the florets can only open to a certain extent due to insufficient elongation of stamen filaments, it is not associated with mutations in any *AP2* homoeologs. The mutation(s) responsible for this pseudo-cleistogamous flowering has not been identified yet.

Proper hydration of spikelet components is crucial for the anther release mechanism. Anthers are usually released during early morning hours, when the plant cells are generally well hydrated (Doorn and Meeteren, 2003, Zajączkowska *et al*. 2021). The expansion of the lodicules facilitates the outward movement of the palea and lemma, leading to the extrusion of anthers. This study showed that anther extrusion was suppressed in the *AP2-D2* mutant compared to that of the wild type and the other two single mutants. The degree of reduction was dose dependent for the mutant allele. This was consistent with the finding that a point mutation in the *AP2-D2* allele has a greater effect on miR172 activity than the other mutant alleles, as suggested by the low energy interaction between *AP2-D2* mRNA and miR172 (Chapter II). Furthermore, double mutant, *AP2-A1/AP2-D2* had a significantly lower anther extrusion rate than the single mutant *AP2-D2* (Chapter III). This implies that allele accumulation, plays a role in reducing the number of anthers being extruded. Based on this information, it can be inferred that *A1* allele and *D2* allele individually have some level of effectiveness in promoting anther retention. When these two alleles are combined, their effects were

amplified, resulting in a stronger impact on anther retention. On the other hand, the *AP2-A1D1* combination, which consists of two weak alleles, does not have the same level of effectiveness in promoting anther retention as the *A1* allele and the *D2* allele combination. These changes in anther retention were consistent with changes in lodicule size.

Reduced interaction between miR172 and its target mRNA from the mutant AP2 homoeologs results in compact spike and reduced culm length

miR172 has perfect or near-perfect complementarity with its target mRNAs, which are usually located in the coding region, and its main mode of action is via mRNA cleavage. High-throughput mapping data and 5' RACE experiments have shown that miR172 can cleave its own primary transcript (pri-miR172), suggesting that the expression of miR172 could be regulated by self-cleavage. miR172 targets include *AP2* and *AP2*-like transcription factors, and the interaction between miR172 and its targets is deeply conserved and has an ancient role in plant developmental regulation (Zhu and Halliwell 2010).

In wheat and barley, miR172 plays a crucial role in regulating spike morphogenesis and flowering. The interaction between miR172 and its target genes, such as *AP2* and *SPL* transcription factors, influences spikelet determinacy, floral development, and plant growth. Specifically, in barley, the suppression of miR172-mediated cleavage of *AP2* mRNA leads to cleistogamous flowering and affects spikelet determinacy. Additionally, in a barley mutant, abnormal spikelet development is observed, indicating the feedback regulation of the *AP2*/miR172 module on *HvSPL* genes. This intricate regulatory network involving miR172, *SPL* genes, and *AP2* transcription factors influences various biological processes, including spikelet development and plant growth phase transition in wheat and barley (Triphati et al. 2018, Volna et al. 2022). Over-

expression of miR172 in rice results in loss of spikelet determinacy and floral organ abnormalities (Zhu et al. 2009).

Barley's cleistogamy alleles (*cly1.b* and *cly1.c*) are derived from natural *HvAP2* gene variants (Nair et al. 2010). Induced Zeocriton (*Zeo*) gene mutants had interesting mutations in *HvAP2*, with three different point mutations identified in the miR172 target site (Houston et al. 2013). The *Zeo1* mutant showed a very compact spike morphology with a remarkable increase in spike density. The phenotype was caused by significantly reduced elongation of rachis internodes. This dense-spike phenotype was much more severe in *Zeo1* than in *Zeo2* (= *cly1.b*) and *Zeo3* (= *cly1.c*). Its severity in *Zeo1* may be due to the greater reduction in the miR172 binding affinity (Houston et al. 2013). The result of wheat *AP2* mRNA interaction with miR172 supports this, where *AP2-D2* had a lower interaction than *AP2-A1* and *AP2-D1*, resulting in a dense-spike morphology (Chapter II, III).

According to Chapter III, mutation at the miR172 target site significantly reduce the rachis and culm internodes. Moreover, there is an indication of positional effect. The positional effect was primarily observed in the upper parts of both tissues. However, the accumulation effect in the double mutant *AP2-A1/AP2-D2* was not observed in either tissue, possibly because the sole effect of the *AP2-D2* allele may be as strong as reaching the reduction limit. On the other hand, there was a clear decrease in the rachis internode elongation and it was dose dependent for each *AP2* mutant allele. Additionally, the weaker alleles *AP2-A1* and *AP2-D1* had a significant additive effect on rachis internode reduction, indicating that they can be used as reliable markers for evaluating the effects of the mutation. Expression analysis in different tissues supports these findings, as the transcript of the *AP2-D2* allele was detected more abundantly in the rachis, culm and immature spikes than in the wild-type allele. The level of transcription appears to be

correlated with the compactness of the spike, with higher transcription levels associated with a more compact spike structure and, consequently, reduced plant height (Simons et al. 2006). The *Zeo1.b* barley mutant with disrupted miR172 targeting of *AP2* exhibits reduced cell division and premature maturation, resulting in stunted growth. It was proposed that miR172 regulation of *AP2* affects the jasmonate pathway, which in turn influences gibberellin-promoted stem growth during the flowering phase (Patil et al. 2019). This shows that the effect of point mutation in the miR172-binding site on the reduction of rachis internode and culm length is common in barley and wheat.

Point mutation in the miR172 target site has pleiotropic effects on other agronomical traits

Studies have shown that point mutations in the miR172 target site of wheat and barley can significantly impact grain and yield related traits. In wheat, these mutations have been linked to changes in spike morphology and grain threshability, with the interaction between miR172 and the *Q* allele being a key factor (Debernardi et al. 2017). In barley, overexpression of miR172 has been found to affect phase transitions and floral meristem determinancy (Curaba et al. 2012). These findings suggest that mutations in the miR172 target site can have a significant impact on the development and yield of wheat and barley.

Although the number of spikelets per spike and grains per spike did not show significant differences across the mutants, a distinct pattern emerged. *AP2-D2* and *AP2-A1/AP2-D2* exhibited the highest number of spikelets per spike and grains per spike. This may be attributed to the compact nature of their spikes. A study by Xie et al. (2017) suggested that increased grain yield per square meter could be attributed to the semi-dwarfing effect of the *Q* allele on plant height, which generally leads to more grains per spikelet. *Q* allele mutation usually results in more grains per spikelet (Xie et al. 2018). It

is possible that the *Cly1/Zeo* ortholog on chromosome 2A is responsible for the shorter spike length and spike compactness, while the number of spikelets per spike remains unaffected (Farris et al. 2014). This observation is supported by the finding that the number of effective spikelets per spike was not reduced in any of the mutants (Chapter III).

Future perspectives for the development of cleistogamous wheat

In summary, *AP2-D2* and *AP2-A1/AP2-D2* mutants had significant effects on anther retention and lodicule size reduction. It is interesting to note that the *AP2-A1D2* mutant exhibits a more profound effect compared to *AP2-D2*, indicating the cumulative effects of these alleles, despite not leading to cleistogamy. Importantly, both the single *AP2-D2* and double *AP2-A1/AP2-D2* mutants demonstrate similar reductions in rachis internode, internode and culm internode length, highlighting the predominant role of the *D2* allele in influencing various agronomic traits.

The accumulation of *AP2* homoeologs with mutations in the miR172 target site can significantly reduce lodicule size and suppress anther extrusion, which is critical for achieving cleistogamy in hexaploid wheat. The presence or absence of the wild-type *AP2-B* homoeolog had no significant effect on phenotype. Combining different miR172 mutations, especially *AP2-B*, will be of particular interest for testing the feasibility of cleistogamy. Debernardi et al. (2020) recently identified a novel point mutation in the miR172 target site of the *AP2-B* homoeolog (*AP2L-B2*) in a dwarf compact spike mutant induced in the hexaploid wheat cv. 'Wedgetail'. The mutant carrying this allele, named *rAp2l-B2*, had smaller lodicules with a significantly reduced (30%) swollen area, although this did not lead to cleistogamy, together with a remarkably compact spike and shorter plant height. This mutant allele is expected to have a strong effect on miR172 activity, as it has a much lower interaction with miR172 than the wild-type *AP2-B* allele.

Combining the *rAp2l-B2* allele with our two mutant alleles, *AP2-A1* and *AP2-D2*, and testing the resulting triple mutant carrying all three mutant homoeologs for cleistogamy and dosage effects of mutant allele combinations is of particular interest.

Therefore, 'complete' cleistogamy, as achieved in barley cultivars, is essential in wheat to improve the initial resistance to FHB. In this respect, the feasibility of developing complete cleistogamy in wheat is the main challenge, apart from the novel insights into the pleiotropic effects of individual mutant *AP2* alleles on other agronomically important traits.

Acknowledgement

I would like to express my sincere gratitude and appreciation to all those who have contributed to the completion of this thesis. First and foremost, I extend my heartfelt thanks to my supervisor, Professor Katsuyuki Kakeda, for giving me the opportunity to partake in this research in his laboratory. I am grateful for his guidance, support, and invaluable expertise throughout this research. His insightful feedback and encouragement have been instrumental in shaping the direction of this research and in writing this thesis.

I would like to extend my sincere gratitude to the two Professors who have also helped me tremendously. Professor Chiharu Nakashima of the Laboratory of Phytopathology, for his guidance, help and expertise in fusarium head blight inoculation and application and for lending me his glasshouse for my experiment. Professor Nobuhito Sekiya of the Laboratory of Global Plant Resource Science for his advice and support in my research on yield and agronomic trait analysis.

I am grateful to the lab technician, Mrs. Miyoko Nitta for her assistance in my experiments. I am indebted to my friends and lab mates of Plant Molecular Genetics and Breeding, especially Mr. Kiyomasha Watanabe and Mr. Hlaing Moe Haine who have provided assistance, and shared their knowledge. Their support has made this journey more enjoyable and enriching. I would like to acknowledge and thank the Japanese Government for the scholarship under MEXT that has provided me with the opportunity to further my studies. I would also like to acknowledge Mie University for providing the avenue, necessary resources, and facilities which have made this research possible.

My deepest appreciation goes to my family for their unwavering love, encouragement, and understanding throughout this endeavor, especially my sons, Kym and JDii for being patient with me. Their belief in my abilities has been a constant source of motivation.

Summary

Cleistogamy or fertilization in closed flowers reduces the risk of fungal infection of the florets at anthesis in Triticeae crops. Cleistogamy in barley (*Hordeum vulgare*) is determined by a single recessive gene at the *Cleistogamy1* (*Cly1*) locus on chromosome 2H. The *Cly1* gene is known to be the barley ortholog of the *Arabidopsis Apetala2* (*AP2*) transcription factor gene. A point mutation within the microRNA172 (miR172) target site of *Cly1* inhibits the binding of miR172 to the target site of the mRNA, resulting in the production of the Cly1 (HvAP2) protein. This protein negatively regulates the development of lodicules, keeping florets closed at anthesis. However, cleistogamy is not evident in hexaploid wheat (*Triticum aestivum*) cultivars. The aim of this study is to develop a cleistogamous wheat which could evade the infection caused by Fusarium head blight and to minimize pollen-mediated gene flow. The present study focused on evaluating the effects of mutations in the wheat *AP2* homoeologs on the potential for cleistogamous flowering.

The initial objective was to identify newly induced mutations in the wheat *AP2* homoeologs, the three homoeologous genes (*AP2-A*, *AP2-B* and *AP2-D*) located on chromosomes 2A, 2B and 2D. The *AP2* mutants were induced from the Japanese winter wheat cultivar 'Kitahonami' by ethyl methanesulfonate (EMS) treatment of the seeds. Three independent mutants carrying novel point mutations within the miR172 target site in *AP2-A* and *AP2-D* were identified and the mutant alleles were designated as *AP2-A1*, *AP2-D1* and *AP2-D2*. However, no point mutations within the miR172 target site were detected in *AP2-B*. These point mutations were distinct from those identified in the cleistogamous alleles *cly1.b* and *cly1.c* of the orthologous barley *Cly1* gene. Field observations showed normal flowering in all mutants. The lodicules of the mutants

swelled during anthesis, however, their sizes exhibited notable variations compared to the wild type. Lodicule depth was decreased in all three mutants, with *AP2-D2* exhibiting the greatest reduction. Lodicule length and width showed a similar trend in *AP2-D2*, however, not in *AP2-A1* or *AP2-D1*. Furthermore, *AP2-D2* had much shorter (compact) spikes compared to *AP2-A1* and *AP2-D1*. The reduced spike length was due to a significant reduction in the length of the rachis (spike) internode. Reduced interaction between mRNA and miR172 at the target site of *AP2-D2* resulted in higher transcript levels that suppressed lodicule development and rachis internode elongation.

A proposed strategy to develop cleistogamous wheat is to accumulate the point mutations in all three *AP2* homoeologs. This study provided insights into the cumulative effects of mutant *AP2* alleles in suppressing open flowering. A precise evaluation of the effects of the mutations was made using near-isogenic lines (NILs). Three single mutants (*AP2-A1*, *AP2-D1* and *AP2-D2*) with two double mutants (*AP2-A1*/*AP2-D1* and *AP2-A1*/*AP2-D2)* were evaluated for the effects on flowering and other agronomic traits under near-isogenic background. Among the three single mutant alleles, *AP2-D2* had the greatest effect on reducing the rate of anther extrusion. Furthermore, the double mutant *AP2-A1*/*AP2-D2* inhibited anther extrusion more than the single mutant *AP2-D2*. Similarly, *AP2-D2* had the greatest effect on reducing lodicule depth, whereas *AP2-A1/AP2-D2* showed a significantly greater reduction in lodicule depth than *AP2-D2*. *AP2-D2* had an additive effect on reducing rachis (spike) internode length, although both *AP2-A1* and *AP2-D1* also had an effect, but less than *AP2-D2*. The double mutant *AP2-A1/AP2-D1* had a stronger effect on reducing rachis internode length than either *AP2-A1* or *AP2-D1*, indicating the cumulative effect of these two alleles. In addition, both single and double mutants carrying the *AP2-D2* allele had shorter culm lengths due to its reduced internode length, suggesting its pleiotropic effect on stem elongation. The *AP2-*

D2 allele showed higher expression levels than the wild type in several floral organs as well as in the rachis and culm.

In conclusion, *AP2-A1/AP2-D2* was evaluated as the most effective genotype in suppressing flower opening, although cleistogamy was not achieved. The study also provided new insights into the pleiotropic effects of individual mutant *AP2* alleles on plant development and agronomic traits in wheat.

References

Alisaac, E, Rathgeb A, Karlovsky P, Mahlein AK (2021) *Fusarium* head blight: Effect of infection timing on spread of *Fusarium graminearum* and spatial distribution of deoxynivalenol within wheat spikes. Microorganisms 9 (1): 79. https://doi.org/10.3390/microorganisms9010079.

Anwar N, Ohta M, Yazawa T, Sato Y, Li C, Tagiri A, Sakuma M, Nussbaumer T, Bregitzer P, Pourkheirandish M, Wu J, Komatsuda T (2018) miR172 downregulates the translation of *cleistogamy 1* in barley. Ann Bot 122: 251–265. https://doi.org/10.1093/aob/mcy058

Beccari G, Arellano C, Covarellia L, Tinia F, Sulyokd M, Cowger C (2018) Effect of wheat infection timing on Fusarium head blight causal agents and secondary metabolites in grain. Int Food Microbiol 290: 214–225.

Bekele B and Dawit W (2018) Review on the Status and Management Strategies of Fusarium Head Blight (*Fusarium Graminearum*) of Wheat. Acad Res J Agri Sci Res 6: 77–88. https://www.academicresearchjournals.org/ARJASR/Index.htm

Cheignon M, Schaever J, Cornier N (1973) Elongation of stamen filament of graminaceae as growth phenomenon. Cr Acad Sci D Nat 276: 319–322

Chen X (2004). A MicroRNA as a Translational Repressor of *APETALA2* in *Arabidopsis* Flower Development. Science N.Y 303: 2022–2025. https://doi.org/10.1126/science.1088060.

Ćosić J, Drezner G, Vrandečić K, Španić V, Poštić J (2008) Effect of *Fusarium culmorum* head blight on yield and DON accumulation. Cereal Research Communications 36: 481–482. https://doi.org/10.1046/j.1439-0434.2000.00557.x

Curaba J, Talbot MJ, Li Z, Helliwell CA (2013) Over-expression of microRNA171 affects phase transitions and floral meristem determinacy in barley. BMC Plant Biol 13: 6– 6. https://doi.org/10.1186/1471-2229-13-6.

Daniell H (2002) Molecular strategies for gene containment in transgenic crops. Nat Biotechnol 20: 5–586. https://doi.org/10.1038/nbt0602-581

Debernardi JM, Lin H, Chuck G, Faris JD, Dubcovsky J (2017) microRNA172 plays a crucial role in wheat spike morphogenesis and grain threshability. Development 144:1966 –1975. https://doi.org/10.1242/dev.146399

Debernardi JM, Greenwood JR, Jean Finnegan E, Jernstedt J, Dubcovsky J (2020) *APETALA 2*-like genes *AP2L2* and *Q* specify lemma identity and axillary floral

meristem development in wheat. Plant J 101:171–187. https://doi.org/10.1111/tpj.14528

Debernardi JM, Woods DP, Li K, Li C, Dubcovsky J (2022) MiR172-*APETALA2-like* genes integrate vernalization and plant age to control flowering time in wheat. PLoS Genet 18: e101057. https://doi.org/10.1371/journal.pgen.1010157

Food and Agriculture Organization of the United Nations (2015) FAO Sta. Available online: https://www.fao.org/faostat/en/#data (accessed on 22 May 2020).

Faris JD and Gill BS (2002) Genomic targeting and high-resolution mapping of the domestication gene *Q* in wheat. Genome 45: 706-18. https://doi.org/10.1139/g02-036.

Guarin JR, Martre P, Ewert F, Webber H, Dueri S, Calderini DF, Reynolds M, Molero G, Miralles DJ, Garcia G, Slafer GA, Giunta, F, Pequeno DN, Stella T, Ahmed M, Alderman PD, Basso B, Berger A, Bindi M, Bracho-Mujica G, Cammarano D, Chen Y, Dumont B, Rezaei, EE, Fereres E, Ferrise R, Gaiser T, Gao Y, García-Vila M, Gayle S, Hochman Z, Hoogenboom G, Hunt, LA, Kersebaum KC, Nendel C, Olesen JE, Palosuo T, Priesack E, Pullens JW, Rodríguez A, Rötter RP, Ramos MR Semenov MA, Senapati N Siebert S, Srivastava AK, Stöckle, CO, Supit I, Tao F, Thorburn PJ, Wang E, Weber TK, Xiao L, Zhang Z, Zhao C, Zhao J, Zhao Z, Zhu Y, Asseng S (2022). Evidence for increasing global wheat yield potential. Environmental Research Letters 17. https://doi.org/10.1088/1748-9326/aca77c.

Graham S, Browne RA (2009) Anther extrusion and Fusarium head blight resistance in European wheat. J Phytopathol 157: 580–582. https://doi.org/10.1111/j.1439-0434.2008.01524.x

Greenwood JR, Finnegan EJ, Watanabe N, Trevaskis B, Swain SM (2017) New alleles of the wheat domestication gene *Q* reveal multiple roles in growth and reproductive development. Development 144: 1959–1965. https://doi.org/10.1242/dev.146407

He X, Lillemo M, Shi J, Wu J, Bjørnstad Å, Belova T, Dreisigacker S, Duveiller E, Singh P (2016) QTL characterization of Fusarium head blight resistance in CIMMYT bread wheat line Soru#1. PLoS One 11: e0158052. https://doi.org/10.1371/journal.pone.0158052

He Z, Joshi AK, Zhang W (2013) Climate Vulnerabilities and Wheat Production. Climate Vulnerability. Understanding and Addressing Threats to Essential Resources. 2: 57–67.

Heslop-Harrison Y, Heslop-Harrison JS (1996) Lodicule function and filament extension in the grasses: Potassium ion movement and tissue specialization. Ann Bot 77: 573–582. https://doi.org/10.1093/aob/77.6.573

Hollingsworth CR, Motteberg CD, Wiersma JV, Atkinson LM (2008) Agronomic and economic responses of spring wheat to management of Fusarium head blight. Plant Dis 92: 1339–1348. https://doi.org/10.1094/PDIS-92-9-1339.

Honda I, Turuspekov Y, Komatsuda T, Watanabe Y (2005) Morphological and physiological analysis of cleistogamy in barley (*Hordeum vulgare*). Physiol Plant 124: 524–531. https://doi.org/10.1111/j.1399-3054.2005.00541.x

Houston K, McKim SM, Comadran J, Bonar N, Druka I, Uzrek N, Cirillo E, Guzy-Wrobelska J, Collins NC, Halpin C, Hansson M, Dockter C, Druka A, Waugh R (2013) Variation in the interaction between alleles of *HvAPETALA2* and microRNA172 determines the density of grains on the barley inflorescence. Proc Natl Acad Sci U S A 110: 16675–16680. https://doi.org/10.1073/pnas.1311681110

Kadar R and Sardar AA (2012) The Effect of Fusarium Graminearum Inoculation on Winter Wheat at ARDS Turda. Bulletin of University of Agricultural Sciences and Veterinary Medicine Cluj-Napoca. Agriculture.

Kirby EJM, Appleyard M (1981) Cereal development guide. National Agricultural Centre Cereal Unit, Stoneleigh, Warwickshire, UK.

Komatsuda T, Nakamura I, Takaiwa F, Oka S (1998) Development of STS markers closely linked to the *vrs1* locus in barley, *Hordeum vulgare*. Genome 41: 680–685

Komura S, Jinno H, Sonoda T, Oono Y, Handa H, Takumi H, Yoshida K, Kobayashi F (2022) Genome sequencing-based coverage analyses facilitate high-resolution detection of deletions linked to phenotypes of gamma-irradiated wheat mutants. BMC Genomics 23: 111.

Kosina, R (2010) On the leafy nature of lodicules in the genus Triticum (Poaceae). *Botanical* Journal of the Linnean Society 164*:* 303–316. https://doi.org/10.1111/j.1095-8339.2010.01090.x

Kubo K, Kawada N, Fujita Masaya, Hatta Koichi, Oda Shunsuke, Nakajima T (2010) Effect of cleistogamy on *Fusarium* head blight resistance in wheat. Breed Sci 60: 405–411. https://doi.org/10.1270/jsbbs.60.405

Kubo K, Fujita M, Kawada N, Nakajima T, Nakamura K, Maejima H, Ushiyama T, Hatta K, Matsunaka H (2013) Minor differences in anther extrusion affect resistance to

Fusarium head blight in wheat. J Phytopathol 161: 308–314. https://doi.org/10.1111/jph.12060

Leflon M, Hüsken A, Kightley SP, Pinochet X (2011) Cleistogamy of oilseed rape, a way to prevent cross-fertilization between adjacent fields. Plant Breeding 130: 338–344. https://doi.org/10.1111/j.1439-0523.2010.01828.x

Livak KJ, and Schmittgen TD (2001) Analysis of relative gene expression data using real-time quantitative PCR and the $2^{-\Delta\Delta}C_T$ method. Methods 25: 402–408.

Lu Q, Lillemo M, Skinnes H, He X, Shi J, Ji F, Dong Y, Bjørnstad A (2013) Anther extrusion and plant height are associated with Type I resistance to Fusarium head blight in bread wheat line 'Shanghai-3/Catbird'. Theor Appl Genet 126: 317–334. https://doi.org/10.1007/s00122-012-1981-9

Lombardo F, Kuroki M, Yao SG, Shimizu H, Ikegaya T, Kimizu M, Ohmori S, Akiyama T, Hayashi T, Yamaguchi T, Koike S, Yatou O, Yoshida H (2016) The *superwoman1-cleistogamy2* mutant is a novel resource for gene containment in rice. Plant Biotechnol J 15: 97–106. https://doi.org/10.1111/pbi.12594

Mehta YR (2014) Wheat and Wheat Production Constraints. In: Wheat Diseases and Their Management. Springer Cham. https://doi.org/10.1007/978-3-319-06465-9_1

Mesterhazy A (1995) Types and components of resistance to *Fusarium* head blight of wheat. Plant Breed 114: 377–386. https://doi:10.1111/j.1439-0523.1995.tb00816

Mesterhazy A, Bartok T, Mirocha CG, Komoroczy R (1999) Nature of wheat resistance to *Fusarium* head blight and the role of deoxynivalenol for breeding. Plant Breed 118: 97–110. https://doi:10.1046/j.1439-0523.1999.118002097

Nair SK, Wang N, Turuspekov Y, Pourkheirandish M, Sinsuwongwat S, Chen G, Sameri M, Tagiri A, Honda I, Watanabe Y, Kanamori H, Wicker T, Stein N, Nagamura Y, Matsumoto T, Komatsuda T (2010) Cleistogamous flowering in barley arises from the suppression of microRNA-guided *HvAP2* mRNA cleavage. Proc Natl Acad Sci U S A 107: 490–495. https://doi.org/10.1073/pnas.0909097107

Nanape AB, Haine HM, Sugimoto K, Kobayashi F, Oono Y, Handa H, Komatsuda T, Kakeda K (2023) Mutations within the miR172 target site of wheat *AP2* homoeologs regulate lodicule size and rachis internode length. Breed Sci (in press). https://doi.org/10.1270/jsbbs.23019

Ni DH, Li J, Duan YB, Yang YC, Wei PC, Xu RF, Li CR, Liang DD, Li H, Song FS, Ni JL, Li L, Yang JB (2014) Identification and utilization of cleistogamy gene *cl7*(*t*) in rice (*Oryza sativa* L.). J Exp Bot 65: 2107–2117. https://doi.org/10.1093/jxb/eru074

Ning S, Wang N, Sakuma S, Pourkheirandish M, Wu J, Matsumoto T, Koba T, Komatsuda T (2013a) Structure, transcription and post-transcriptional regulation of the bread wheat orthologs of the barley cleistogamy gene *Cly1*. Theor Appl Genet 126: 1273–1283. https://doi.org/10.1007/s00122-013-2052-6

Ning S, Wang N, Sakuma S, Pourkheirandish M, Koba T, Komatsuda T (2013b) Variation in the wheat *AP2* homoeologs, the genes underlying lodicule development. Breed Sci 63: 255–266. https://doi.org/10.1270/jsbbs.63.255

Ohmori S, Tabuchi H, Yatou O, Yoshida H (2012) Agronomic traits and gene containment capability of cleistogamous rice lines with the *superwoman1-cleistogamy* mutation. Breed Sci 62:124–132. https://doi.org/10.1270/jsbbs.62.124

Ohmori S, Koike S, Hayashi T, Yamaguchi T, Kuroki M, Yoshida H (2018) The cleistogamy of the *superwoman1-cleistogamy1* mutation is sensitive to low temperatures during the lodicule-forming stage. Breed Sci.68(4): 432–441. https://doi.org/10.1270/jsbbs.18028

Patil V, McDermott HI, McAllister T, Cummins M, Silva JC, Mollison E, Meikle R, Morris J, Hedley PE, Waugh R, Dockter C, Hansson M, McKim SM (2019) APETALA2 control of barley internode elongation. Development 146: dev170373. https://doi.org/10.1242/dev.170373

Pierre J, Fargue A, Picault H, Pinochet X, Renard M (2007) Methods to study the advantages of cleistogamy in oilseed rape in limiting unwanted gene flow. Euphytica 151: 1–13. https://doi.org/10.1007/s10681-005-9005-3

Polišenská I, Vaculová K, Jirsa O, Sedláčková I, Frydrych J (2020) The effect of Fusarium culmorum on yield and grain characteristics of winter wheat cultivars. Zemdirbyste-agriculture 107: 113–122. https://doi.org/10.13080/z-a.2020.107.015

Purnell M (2016) Slow turnaround for the wheat industry. African Journal 2: 6–13. https://hdl.handle.net/10520/EJC195123

Riaz MW, Lu J, Shah L, Yang L, Chen C, Mei XD, Xue L, Manzoor MA, Abdullah M, Rehman S, Si H, Ma C (2021) Expansion and Molecular Characterization of *AP2/ERF* Gene Family in Wheat (*Triticum aestivum* L.). Front Genet 12: 632155. https://doi.org/10.3389/fgene.2021.632155

Rehmsmeier M, Steffen P, Höchsmann M, Giegerich R (2004) Fast and effective prediction of microRNA/target duplexes. RNA 10: 1507–1517.

Salgado JD, Wallhead M, Madden LV, Paul P A (2011) Grain Harvesting Strategies to Minimize Grain Quality Losses Due to Fusarium Head Blight in Wheat. Plant Dis 95: 1448–1457. https://doi.org/10.1094/PDIS-04-11-0309

Salgado J D, Laurence MV, Pierce PA (2015) Quantifying the effects of fusarium head blight on grain yield and test weight in soft red winter wheat. Phytopathology 105: 295–306. https://doi.org/10.1094/PHYTO-08-14-0215-R

Saunders R (2024), *flower*. Encyplopaedia Britannica. https://www.britannica.com/science/flower. Accessed 27 April 2024

Schaafsma AW and Tamburic-Ilincic L (2005) Effect of Seeding Rate and Seed Treatment Fungicides on Agronomic Performance, Fusarium Head Blight Symptoms, and DON Accumulation in Two Winter Wheats. Plant Dis 89 10: 1109–1113. https://doi.org/10.1094/PD-89-1109.

Sharma I, Tyagi B, Singh G, Venkatesh K, Gupta OP (2015) Enhancing wheat production- A global perspective. The Indian Journal of Agricultural Sciences 85: 3–13.

Shoesmith JR, Solomon CU, Yang X, Wilkinson LG, Sheldrick S, van Eijden E, Couwenberg S, Pugh LM, Eskan M, Stephens J, Barakate A, Drea S, Houston K, Tucker MR, McKim SM (2021) APETALA2 functions as a temporal factor together with BLADE-ON-PETIOLE2 and MADS29 to control flower and grain development in barley. Development 148: dev194894. https://doi.org/10.1242/dev.194894

Simons KJ, Fellers JP, Trick HN, Zhang Z, Tai YS, Gill BS, Faris JD (2006) Molecular characterization of the major wheat domestication gene *Q*. Genetics 172: 547–555. https://doi.org/10.1534/genetics.105.044727

Sormacheva I, Golovnina K, Vavilova V, Kosuge K, Watanabe N, Blinov AG, Goncharov NP (2014) *Q* gene variability in wheat species with different spike morphology. Genet Resour and Crop Evol. 62: 837–852. https://doi.org/10.1007/s10722-014-0195-1

Sparks CA, Jones HD (2004) Transformation of Wheat by Biolistics. Transgenic Crops of the World. Springer, Dordrecht. https://doi.org/10.1007/978-1-4020-2333-0_2

Supronienė S, Mankevičienė A, Kadžienė G, Kačergius A, Feiza V, Feiziene D., Semaškienė, R, Dabkevičius Z, Tamošiu¯nas K (2012) The impact of tillage and fertilization on Fusarium infection and mycotoxin production in wheat grains.

Zemdirbyste-agriculture 99: 265–272. https://api.semanticscholar.org/CorpusID:38125748

Tang C, Zhang H, Zhang P, Ma Y, Cao M, Hu H, Shah FA, Zhao W, Li M, Wu L (2019) iTRAQ-based quantitative proteome analysis reveals metabolic changes between a cleistogamous wheat mutant and its wild-type wheat counterpart. PeerJ 7: e7104. https://doi.org/10.7717/peerj.7104

Tripathi, RK, Bregitzer, P, Singh, J (2018) Genome-wide analysis of the SPL/miR156 module and its interaction with the AP2/miR172 unit in barley. Sci Rep 8: 7085. https://doi.org/10.1038/s41598-018-25349-0

Turuspekov Y, Mano Y, Honda I, Kawada N, Watanabe Y, Komatsuda T (2004) Identification and mapping of cleistogamy genes in barley. Theor Appl Genet 109: 480–487. https://doi.org/10.1007/s00122-004-1673-1.

Turuspekov Y, Kawada N, Honda I, Watanabe Y, Komatsuda T (2005) Identification and mapping of a QTL for rachis internode length associated with cleistogamy in barley. Plant Breed 124: 542–545. https://doi.org/10.1111/j.1439-0523.2005.01161.x

Ueno K, Itoh H (1997) Cleistogamy in wheat: genetic control and the effect of environmental conditions. Cereal Res Commun 25: 185–189. https://doi.org/10.1007/BF03543455

van Doorn WG, van Meeteren U (2003) Flower opening and closure. a review. J Exp Bot 54: 1801–1812. https://doi.org/10.1093/jxb/erg213

Varani G and McClain WH (2000) The G·U wobble base pair: A fundamental building block of RNA structure crucial to RNA function in diverse biological systems. EMBO Reports 1: 18–23.

Volná A, Martin B, Petr P, Vladimír Š, Jiří Č (2022) What Do We Know about Barley miRNAs? Int J of Mol Sci 23: 14755. https://doi.org/10.3390/ijms232314755

Wang N, Ning S, Pourkheirandish M, Honda I, Komatsuda T (2013) An alternative mechanism for cleistogamy in barley. Theor Appl Genet 126: 2753–2762. https://doi.org/10.1007/s00122-013-2169-7

Wang N, Ning S, Wu J, Tagiri A, Komatsuda T (2015) An epiallele at *cly1* affects the expression of floret closing (cleistogamy) in barley. Genetics 199: 95–104. https://doi.org/10.1534/genetics.114.171652

Wang N, Kakeda K, Tomokazu M, Liu C, Yoshida M, Kawada N, Komatsuda T (2021) A novel mutant allele at the *Cleistogamy* 1 locus in barley. Theor Appl Genet 134: 3183–3193. https://doi.org/10.1007/s00122-021-03884-1

Wang R, Chen J, Anderson JA, Zhang J, Zhao W, Wheeler J, Klassen N, See DR, Dong Y (2017) Genome-wide association mapping of Fusarium head blight resistance in spring wheat lines developed in the Pacific Northwest and CIMMYT. Phytopathology 2107: 1486–1495. https://doi.org/10.1094/PHYTO-02-17-0073-R

Wegulo SN, Baenziger PS, Nopsa JH, Bockus WW, Adams HH (2015) Management of Fusarium head blight of wheat and barley. Crop Production 100: 763–773. https://doi.org/10.1016/j.cropro.2015.02.025

Xie Q, Li N, Yang Y, Lv Y, Yao, H, Wei R, Sparkes DL, Ma Z (2018) Pleiotropic effects of the wheat domestication gene *Q* on yield and grain morphology. Planta 247: 1089–1098.

Xu BJ, Chen Q, Zheng T, Jiang YF, Qiao YY, Guo ZR, Cao YL, Wang Y, Zhang YZ, Zong LJ, Zhu J, Liu CH, Jiang QT, Lan XJ, Ma J, Wang JR, Zheng YL, Wei YM, Qi PF (2018) An overexpressed *Q* allele leads to increased spike density and improved processing quality in common wheat (*Triticum aestivum*). G3 (Bethesda) 8: 771–778. https://doi.org/10.1534/g3.117.300562

Yin J (2002) On flowering characters and structural changes of lodicule during the flowering in wheat.

Yoshida H (2012) Is the lodicule a petal: molecular evidence? Plant Sci 184: 121–8.

Yoshida M, Nakajima (2010) Deoxynivalenol and nivalenol accumulation in wheat infected with *Fusarium graminearum* during grain development. Phytopathology 100(8): 763–73. https://doi.org/10.1094/PHYTO-100-8-0763.

Yoshida M, Kawada N, Nakajima T (2007) Effect of infection timing on Fusarium head blight and mycotoxin accumulation in open- and closed-flowering barley. Phytopathology 97: 1054–1062. https://doi.org/10.1094/PHYTO-97-9-1054

Yoshida M, Kawada N, Tohnooka T (2005) Effect of row type, flowering type and several other spike characters on resistance to Fusarium head blight in barley. Euphytica 141: 217–227. https://doi.org/10.1007/s10681-005-7008-8

Zadoks JC, Changt TT, Konzak CF (1974) A decimal code for the growth stages of cereals. Weed Res 14: 415–421.

Zajączkowska U, Denisow B, Łotocka B, Dołkin-Lewko A, Rakoczy-Trojanowska M (2021) Spikelet movements, anther extrusion and pollen production in wheat

cultivars with contrasting tendencies to cleistogamy. BMC Plant Biol 21:136. https://doi.org/10.1186/s12870-021-02917-7

Zhang H, Zhang J, Yan J, Gou F, Mao Y, Tang G, Botella JR, Zhu J (2017) Short tandem target mimic rice lines uncover functions of miRNAs in regulating important agronomic traits. Proc Natl Acad Sci 114: 5277–5282. https://doi.org/10.1073/pnas.1703752114

Zhang J, Xiong H, Guo H, Li Y, Xie X, Xie Y, Zhao L, Gu J, Zhao S, Ding Y, Liu L (2022) Identification of the *Q* gene playing a role in spike morphology variation in wheat mutants and its regulatory network. Front Plant Sci 12: 807731. https://doi.org/10.3389/fpls.2021.807731

Zhang Z, Li A, Song G, Geng S, Gill BS, Faris JD, Mao L (2019) Comprehensive analysis of *Q* gene near-isogenic lines reveals key molecular pathways for wheat domestication and improvement. Plant J 102: 299–310. https://doi.org/10.1111/tpj.14624

Zhao K, Xiao J, Liu Y, Chen S, Yuan C, Cao A, You FM, Yang D, An S, Wang H, Wang X (2018) *Rht23* (*5Dq*) likely encodes a *Q* homeologue with pleiotropic effects on plant height and spike compactness. Theor Appl Genet 131: 1825–1834. https://doi.org/10.1007/s00122-018-3115-5

Zhao Q, Sun C, Liu D, Hao Y, You C (2015) Ectopic expression of the apple *Md-miR172e* gene alters flowering time and floral organ identity in *Arabidopsis*. Plant Cell, Tiss Organ Cult 123: 535 – 546. https://doi.org/10.1007/s11240-015-0857-5.

Zhao Y, Ma R, Xu D, Bi H, Xia Z, Peng H (2019) Genome-wide identification and analysis of the *AP2* transcription factor gene family in wheat (*Triticum aestivum* L.). Front Plant Sci 10: 1286. https://doi.org/10.3389/fpls.2019.01286

Zhu QH, Upadhyaya NM, Gubler F, Helliwell CA (2009) Over-expression of miR172 causes loss of spikelet determinacy and floral organ abnormalities in rice (*Oryza sativa*). https://doi.org/10.1186/1471-2229-9-149

Zhu QH and Helliwell CA (2011) Regulation of flowering time and floral patterning by miR172. J Exp Bot 62: 487–495. https://doi.org/10.1093/jxb/erq295

Jung J, Lee S, Yun J, Le, Park C (2014) The miR172 target TOE3 represses *AGAMOUS* expression during *Arabidopsis* floral patterning. Plant Sci 215: 29–38. https://doi.10.1016/j.plantsci.2013.10.010